

# Quantum Imaging

Yanhua Shih

Department of Physics

University of Maryland, Baltimore County,

Baltimore, MD 21250

**Abstract:** One of the most surprising consequences of quantum mechanics is the entanglement of two or more distant particles. Although questions regarding fundamental issues of quantum theory still exist, quantum entanglement has started to play important roles in practical engineering applications. Quantum imaging is one of these exciting areas. Quantum imaging has demonstrated two peculiar features: (1) reproducing “ghost” images in a “nonlocal” manner, and (2) enhancing the spatial resolution of imaging beyond the diffraction limit. In this article, we start with the review of classical imaging to establish the basic concepts and formalisms of imaging. We then analyze two-photon imaging with particular emphasis on the physics of spatial resolution enhancement and the “ghost” imaging phenomenon.

## 1 Introduction

Quantum mechanics remarkably allows for the entanglement of two or more distant particles. In a maximally entangled two-particle system, the value of an observable for each particle is completely undefined while the correlation between the two can be uniquely determined, *despite the distance between them*. In other words, each of the two subsystems may have *completely random values* or *all possible values* for some physical observable in the course of their propagation, but the correlations of the two subsystems are determined uniquely and with certainty through the measurement of joint-detection events [1]. Although questions regarding fundamental issues of quantum theory still exist, quantum entanglement has started to play important roles in practical engineering applications. Quantum imaging is one of these exciting areas.

The first quantum imaging experiment was demonstrated by Pittman *et al.* in 1995 [2], inspired by the theory of Klyshko [3]. The experiment was immediately named “ghost imaging” due to its surprising nonlocal feature. The important physics demonstrated in that experiment, nevertheless, may not be the “ghost.” Indeed, the original purpose of the experiment was to study and to test the two-particle EPR correlation in position and in momentum for an entangled two-photon system [4][5][6][7]. The experiments of ghost imaging and ghost interference [8] together stimulated the foundation of quantum imaging in terms of geometrical and physical optics.

Entangled multi-photon systems were later introduced to lithography for sub-diffraction-limited imaging [9]. In 2000, Boto *et al.* proposed a “noon” state and approved that the entangled N-photon system may improve the spatial resolution of an imaging system by a factor of N, despite the Rayleigh diffraction limit. The working principle of quantum lithography was experimentally demonstrated by D’Angelo *et al.* in 2001 [10] by taking advantage of an entangled two-photon state of spontaneous parametric down-conversion (SPDC). Due to the lack of a two-photon absorber, the joint-detection measurement in that experiment was on the Fourier transform plane rather than on the image plane. The observed Fourier transform of the object function is the same as the one produced by classical light of wavelength  $\lambda/2$ . It was implicit in Ref.[10] that a second Fourier transform, by inserting a second lens in that experimental setup, would transfer the Fourier transform of the object onto its image plane, thus giving an image with doubled spatial resolution despite the Rayleigh diffraction limit.

Quantum imaging has so far demonstrated two peculiar features: (1) reproducing ghost images in a “nonlocal” manner, and (2) enhancing the spatial resolution of imaging beyond the diffraction limit. Both the nonlocal behavior observed in the ghost imaging experiment and the apparent violation of the uncertainty principle explored in the quantum lithography experiment are due to the two-photon coherent effect, which involves the superposition of two-photon amplitudes, a nonclassical entity corresponding to different yet indistinguishable alternative ways of triggering a joint-detection event, under the framework of quantum theory of photodetection [11].

The nonlocal superposition of two-photon states may never be understood classically. Classical attempts, however, have never stopped in the history of EPR studies. Bennink *et al.* demonstrated an interesting experiment in 2002 [12]. In that experiment, two co-rotated laser beams produced a projection shadow of an object mask through coincidence measurements. Instead of having a superposition of a large number of two-photon probability *amplitudes*, Bennink used two correlated laser beams (imagine two back to back lasers) to simulate each two-photon *probability* one at a time. If the laser beam propagating in the object arm is blocked by the mask at a certain rotating angle, there would be no coincidence in that angle and consequently the corresponding “position” in the nonlocal “image” plane, defined by the correlated laser beams which were propagated to a different directions. The block-unblock of the correlated laser beams projected a shadow of the object mask in coincidences. Interestingly, this experiment has excited a number of discussions concerning certain historical realistic models of EPR. Despite the fact that the measured correlation by Bennink *et al.* is not the EPR correlation in momentum and, simultaneously, in position but rather a trivial “momentum-momentum” correlation defined by the two co-rotating laser beams on their Fourier transform planes, this experiment is a good example in distinguishing a two-photon image from a correlated projection shadow [6][7].

Thermal light ghost imaging was another challenge. In 2004, Gatti *et al.* [13], Wang *et al.* [14], and Zhu *et al.* [15] proposed ghost imaging by replacing entangled state with chaotic thermal radiation. A question about ghost imaging is then naturally raised: Is ghost imaging a quantum effect if it can be simulated by “classical” light? Thermal light ghost imaging is based on the second-order spatial correlation of thermal radiation. In fact, two-photon correlation of thermal radiation is not a new observation. Hanbury-Brown and Twiss (HBT) demonstrated the intensity spatial correlation of thermal light in 1956 [16]. Differing from entangled states, the maximum correlation in thermal radiation is 50%, which means 33% visibility of intensity modulation at most. Nevertheless, thermal light is a useful candidate for ghost imaging in certain applications. Recently, a number of experiments successfully demonstrated certain interesting features of ghost imaging by using chaotic light [17] [18][19][20].

The HBT experiment was successfully interpreted as statistical correlation of intensity fluctuations. In HBT, the measurement is in far-field (Fourier transform plane). The measured two intensities have the same fluctuations while the two photodetectors receive the same mode and thus yield maximum correlation

$$\langle I_1 I_2 \rangle = \bar{I}_1 \bar{I}_2 + \langle \Delta I_1 \Delta I_2 \rangle. \quad (1)$$

When the two photodetector receive different modes, however, the intensities have different fluctuations, the measurement yields  $\langle \Delta I_1 \Delta I_2 \rangle = 0$  and gives  $\langle I_1 I_2 \rangle = \bar{I}_1 \bar{I}_2$ . One type of the HBT experiments explored the partial (50% ) spatial correlation  $\langle I_1 I_2 \rangle \sim 1 + \delta[(\vec{\rho}_1 - \vec{\rho}_2)(\Delta\theta)]$  of the thermal radiation field, where  $\vec{\rho}_j$  is the transverse coordinate of the  $j^{th}$  photodetector and  $\Delta\theta$  is the angular size of the source. This result has been applied in Astronomy for measuring the angular size of stars.

Although Eq. (1) gives a reasonable explanation to the far-field HBT phenomena, the theory of statistical correlation of intensity fluctuation may not work for ghost imaging: (1) this theory fails to provide adequate interpretation for ghost imaging of entangled states. The visibility of ghost image of entangled two-photon state is 100% which means a 100% correlation, i.e.,  $\langle I_1 I_2 \rangle \sim \delta(\vec{\rho}_1 - \vec{\rho}_2/m)$ , where  $m$  is the magnification factor of imaging. If one insists on

Eq. (1), the mean intensities  $\bar{I}_1$  and  $\bar{I}_2$  must be zero. Otherwise Eq. (1) leads to non-physical conclusions. The measurements, however, never yield zero mean values of  $\bar{I}_1$  and  $\bar{I}_2$  in any circumstances. (2) Scarcelli *et al.* recently demonstrated a lens-less “near-field” ghost imaging of chaotic radiation [18] and pointed out that the theory of statistical correlation of intensity fluctuation does not work for their experiment. Differing from HBT in which the measurement is in far-field, Scarcelli’s experiment is in near-field. In near-field, for each point on the detection plane, a point photodetector receives a large number of ( $N$ ) modes in the measurement. The ratio between joint-detections triggered by “identical mode” and joint-detections triggered by “different modes” is  $N/N^2$ . For a large  $N$ , the contributions from “identical mode” is negligible and thus  $\langle \Delta I_1 \Delta I_2 \rangle = 0$ . Therefore, the classical idea of statistical correlation of intensity fluctuations will not work in the multi-mode case, as we know that different modes of chaotic light fluctuate randomly and independently. On the other hand, Scarcelli *et al.* proved a successful alternative interpretation based on the quantum theory of two-photon interference.

It is interesting to see that the concept of two-photon coherence is applicable to both “classical” and “quantum” light. Although, two-photon superposition is a new concept benefited from recent research of entangled states [4], the concept is not restricted to the entangled states. The concept is generally true and applicable to any radiation, including “classical” thermal light. It is then reasonable to ask: What is the difference between entangled two-photon imaging and thermal light two-photon imaging? To what extent can two-photon correlation of chaotic radiation replace the roles of entangled states? Can two-photon imaging of chaotic light improve imaging resolution beyond the classical limit? Another reasonable question may trap us into an enduring debate: Is thermal light ghost imaging “classical” or “quantum”? Is ghost imaging, in general, “classical” or “quantum”?

This article attempts to provide answers to these hotly debated questions. To this end, we start with the review of classical imaging. The treatment of classical imaging may serve to establish the basic concept and formalism we are going to use in the rest of this article. We then analyze two-photon imaging with particular emphasis on the physics of spatial resolution enhancement and the “ghost” imaging phenomenon.

## 2 Imaging and Spatial Resolution

The concept of imaging is well defined in classical optics. Fig. 1 schematically illustrates a standard imaging setup. A lens of finite size is used to image the object onto an image plane

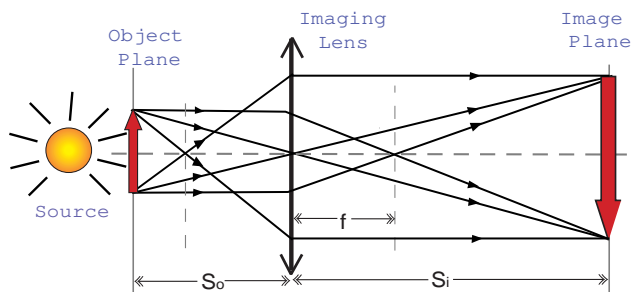


Figure 1: Imaging: a lens produces an *image* of an object in the plane defined by the Gaussian thin lens equation  $1/s_i + 1/s_o = 1/f$ . The concept of an image is based on the existence of a point-to-point relationship between the object plane and the image plane.

which is defined by the “Gaussian thin lens equation”

$$\frac{1}{s_i} + \frac{1}{s_o} = \frac{1}{f} \quad (2)$$

where  $s_o$  is the distance between object and lens,  $f$  is the focal length of the lens and  $s_i$  is the distance between lens and image plane. If light always follows the laws of geometrical optics, the image plane and the object plane would have a perfect point-to-point correspondence, which means a perfect image of the object, either magnified or demagnified. Mathematically, a perfect image is the result of a convolution of the object distribution function  $f(\vec{\rho}_o)$  and a  $\delta$ -function. The  $\delta$ -function characterizes the perfect point-to-point relationship between the object plane and the image plane:

$$F(\vec{\rho}_i) = \int_{obj} d\vec{\rho}_o f(\vec{\rho}_o) \delta(\vec{\rho}_o + \vec{\rho}_i/m) \quad (3)$$

where  $\vec{\rho}_o$  and  $\vec{\rho}_i$  are 2-D vectors of the transverse coordinate in the object plane and the image plane, respectively, and  $m$  is the magnification factor.

Unfortunately, light behaves like a wave. The diffraction effect turns the point-to-point correspondence into a point-to-“spot” relationship. The  $\delta$ -function in the convolution of Eq. (3) will be replaced by a point-spread function.

$$F(\vec{\rho}_i) = \int_{obj} d\vec{\rho}_o f(\vec{\rho}_o) \text{somb}\left[\frac{R}{s_o} \frac{\omega}{c} |\vec{\rho}_o + \vec{\rho}_i/m|\right] \quad (4)$$

where

$$\text{somb}(x) = \frac{2J_1(x)}{x},$$

and  $J_1(x)$  is the first-order Bessel function,  $R$  is the radius of the imaging lens. The finite size of the spot, which is defined by the point-spread function, determines the spatial resolution of the imaging setup, and thus, limits the ability of making demagnified images. It is clear from Eq. (4), the use of larger imaging lens and shorter wavelength light source will result in a narrower point-spread function. To improve the spatial resolution, one of the efforts in the lithography industry is the use of shorter wavelengths. This effort is, however, limited to a certain level because of the lack of lenses effectively working beyond a certain “cutoff” wavelength.

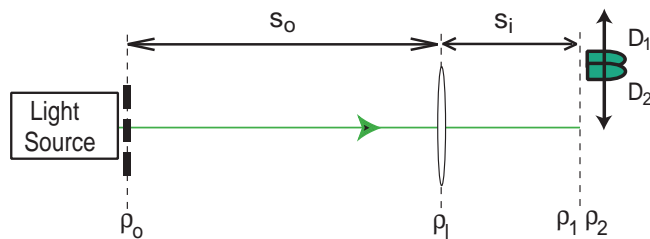


Figure 2: Typical imaging setup. A lens of finite size is used to produce a demagnified image of a object with limited spatial resolution. Replacing classical light with an entangled  $N$ -photon system, the spatial resolution can be improved by a factor of  $N$ , despite the Rayleigh diffraction limit.

Eq. (4) imposes a diffraction limited spatial resolution on an imaging system while the aperture size of the imaging system and the wavelength of the light source are both fixed. This limit is fundamental in both classical optics and in quantum mechanics. Any violation would be considered as the violation of the uncertainty principle.

Surprisingly, the use of quantum entangled states gives a different result: by replacing classical light sources in Fig. 2 with entangled  $N$ -photon states, the spatial resolution of the image can be improved by a factor of  $N$ , despite the Rayleigh diffraction limit. Is this a violation of the uncertainty principle? The answer is no! The uncertainty relation for an entangled  $N$ -particle system is radically different from that for  $N$  independent particles. In terms of the

terminology of imaging, what we have found is that the  $somb(x)$  in the convolution of Eq. (4) has a different form in the case of an entangled state. For example, an entangled two-photon system has

$$x = \frac{R}{s_o} \frac{2\omega}{c} |\vec{\rho}_o + \vec{\rho}_i/m|,$$

and thus yields a twice narrower point-spread function and results in a doubling spatial resolution for imaging.

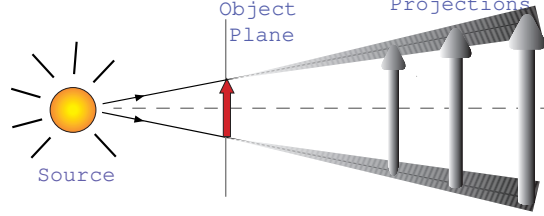


Figure 3: Projection: a light source illuminates an object and no image forming system is present, no image plane is defined, and only projections, or shadows, of the object can be observed.

It should be emphasized that one must not confuse a “projection” with an image. A projection is the shadow of an object, which is obviously different from the image of an object. Fig. 3 distinguishes a projection shadow from an image. The difference is more obvious when the projection shadow is accumulated one-ray-at-a-time, as Bennink *et al.* did in their experiment [12]. In a projection, the object-shadow correspondence is essentially a “momentum” correspondence, which is defined by the propagation direction of the light rays. This point will be emphasized again in the section of ghost imaging.

### 3 Classical Imaging

We now analyze classical imaging. The analysis starts from the propagation of the field from the object plane to the image plane. In classical optics, such propagation is described by an optical transfer function  $h(\mathbf{r} - \mathbf{r}_0, t - t_0)$ , which accounts for the propagation of all modes of the field. In view of our quantum optics approach, we prefer to work with the single-mode propagator  $g(\mathbf{k}, \mathbf{r} - \mathbf{r}_0, t - t_0)$  and its Fourier transform [21][22]. It is convenient to write the field  $E(\mathbf{r}, t)$  in terms of its longitudinal ( $z$ ) and transverse ( $\vec{\rho}$ ) coordinates under the Fresnel paraxial approximation [21]:

$$E(\vec{\rho}, z, t) = \int d\omega d\vec{\kappa} \tilde{E}(\vec{\kappa}, \omega) g(\vec{\kappa}, \omega; \vec{\rho}, z) e^{-i\omega t} \quad (5)$$

where  $\tilde{E}(\omega, \vec{\kappa})$  is the complex amplitude of frequency  $\omega$  and transverse wave-vector  $\vec{\kappa}$ . In Eq. (5) we have taken  $z_0 = 0$  and  $t_0 = 0$  at the object plane as usual. To simplify the notation, we have assumed one polarization.

Based on the experimental setup of Fig. 2,  $g(\vec{\kappa}, \omega; \vec{\rho}, z)$  is found to be [21][22]

$$\begin{aligned} & g(\vec{\kappa}, \omega; \vec{\rho}_i, s_o + s_i) \\ &= \int_{obj} d\vec{\rho}_o \int_{lens} d\vec{\rho}_l \left\{ A(\vec{\rho}_o) e^{i\vec{\kappa} \cdot \vec{\rho}_o} \right\} \left\{ \frac{-i\omega}{2\pi c} \frac{e^{i\frac{\omega}{c}s_o}}{s_o} e^{i\frac{\omega}{2cs_o} |\vec{\rho}_l - \vec{\rho}_o|^2} \right\} \left\{ e^{-i\frac{\omega}{2cs_i} |\vec{\rho}_l|^2} \right\} \\ & \times \left\{ \frac{-i\omega}{2\pi c} \frac{e^{i\frac{\omega}{c}s_i}}{s_i} e^{i\frac{\omega}{2cs_i} |\vec{\rho}_i - \vec{\rho}_l|^2} \right\} \end{aligned} \quad (6)$$

where  $\vec{\rho}_o$ ,  $\vec{\rho}_l$ , and  $\vec{\rho}_i$  are two-dimensional vectors defined, respectively, on the object, the lens, and the image planes. The first curly bracket includes the aperture function  $A(\vec{\rho}_o)$  of the

object and the phase factor  $e^{i\vec{\kappa}\cdot\vec{\rho}_o}$  contributed to the object plane by each transverse mode  $\vec{\kappa}$ . The terms in the second and the fourth curly brackets describe free-space Fresnel propagation-diffraction from the source/object plane to the imaging lens, and from the imaging lens to the detection plane, respectively. The Fresnel propagator includes a spherical wave function  $e^{i\frac{\omega}{c}(z_j-z_k)}/(z_j-z_k)$  and a Fresnel phase factor  $e^{i\omega|\vec{\rho}_j-\vec{\rho}_k|^2/2c(z_j-z_k)}$ . The third curly bracket adds the phase factor introduced by the imaging lens. A brief review of Fresnel diffraction-propagation is given in Appendix A.

We now rewrite Eq. (6) into the following form

$$\begin{aligned} & g(\vec{\kappa}, \omega; \vec{\rho}_i, z = s_o + s_i) \\ &= \frac{-\omega^2}{(2\pi c)^2 s_o s_i} e^{i\frac{\omega}{c}(s_o+s_i)} e^{i\frac{\omega}{2cs_i}|\vec{\rho}_i|^2} \int_{obj} d\vec{\rho}_o A(\vec{\rho}_o) e^{i\frac{\omega}{2cs_o}|\vec{\rho}_o|^2} e^{i\vec{\kappa}\cdot\vec{\rho}_o} \\ & \quad \times \int_{lens} d\vec{\rho}_l e^{i\frac{\omega}{2c}[\frac{1}{s_o}+\frac{1}{s_i}-\frac{1}{f}]|\vec{\rho}_l|^2} e^{-i\frac{\omega}{c}(\frac{\vec{\rho}_o+\vec{\rho}_i}{s_o+\frac{\vec{\rho}_i}{m}})\cdot\vec{\rho}_l}. \end{aligned} \quad (7)$$

The image plane is defined by the Gaussian thin-lens equation of Eq. (2). Hence, the second integral in Eq. (7) simplifies and gives, for a finite sized lens of radius  $R$ , the so called point-spread function of the imaging system:  $somb(x) = 2J_1(x)/x$ , where  $x = [\frac{R}{s_o} \frac{\omega}{c} |\vec{\rho}_o + \rho_i/m|]$ ,  $J_1(x)$  is the first-order Bessel function and  $m = s_i/s_o$  is the magnification of the imaging system.

Substituting the result of Eqs. (7) into Eq. (5) enables one to obtain the classical self-correlation of the field, or, equivalently, the intensity on the image plane

$$I(\vec{\rho}_i, z_i, t_i) = \langle E^*(\vec{\rho}_i, z_i, t_i) E(\vec{\rho}_i, z_i, t_i) \rangle \quad (8)$$

where  $\langle \dots \rangle$  denotes an ensemble average. We assume monochromatic light for classical imaging as usual [24].

Case (I): *incoherent imaging*. The ensemble average of  $\langle \tilde{E}^*(\vec{\kappa}, \omega) \tilde{E}(\vec{\kappa}', \omega) \rangle$  yields zeros except when  $\vec{\kappa} = \vec{\kappa}'$ . The image is thus

$$I(\vec{\rho}_i) \propto \int d\vec{\rho}_o |A(\vec{\rho}_o)|^2 |somb[\frac{R}{s_o} \frac{\omega}{c} |\vec{\rho}_o + \frac{\vec{\rho}_i}{m}|]|^2. \quad (9)$$

An incoherent image, magnified by a factor of  $m$ , is thus given by the convolution between the squared moduli of the object aperture function and the point-spread function. The spatial resolution of the image is thus determined by the finite width of the  $|somb|^2$ -function.

Case (II): *coherent imaging*. The coherent superposition of the  $\vec{\kappa}$  modes in both  $E^*(\vec{\rho}_i, \tau)$  and  $E(\vec{\rho}_i, \tau)$  results in a wavepacket. The image, or the intensity distribution on the image plane, is thus

$$I(\vec{\rho}_i) \propto \left| \int_{obj} d\vec{\rho}_o A(\vec{\rho}_o) e^{i\frac{\omega}{2cs_o}|\vec{\rho}_o|^2} somb[\frac{R}{s_o} \frac{\omega}{c} |\vec{\rho}_o + \frac{\vec{\rho}_i}{m}|] \right|^2. \quad (10)$$

A coherent image, magnified by a factor of  $m$ , is thus given by the squared modulus of the convolution between the object aperture function (multiplied by a Fresnel phase factor) and the point-spread function.

For  $s_i < s_o$  and  $s_o > f$ , both Eqs. (9) and (10) describe a real demagnified inverted image. In both cases, a narrower  $somb$ -function yields a higher spatial resolution. Thus, the use of shorter wavelengths allows for the improving of the spatial resolution of an imaging system.

## 4 Two-photon Imaging

To demonstrate the working principle of quantum imaging, we replace the classical light source in Fig. 2 with an entangled two-photon source such as spontaneous parametric down-conversion (SPDC) [23][4] and replace the ordinary film with a two-photon absorber, which is

sensitive to two-photon transition only, on the image plane. We will show that, in the same experimental setup of Fig. 2, an entangled two-photon system gives rise, on a two-photon absorber, to a point-spread function twice narrower than the one obtained in classical imaging at the same wavelength. Then, without employing shorter wavelengths, entangled two-photon states improve the spatial resolution of a *two-photon image* by a factor of 2.

What is special about the entangled two-photon state of SPDC? Let us imagine a measurement in which we place two point-like single photon counting detectors ( $D_1$  and  $D_2$ ) on the output surface of an SPDC crystal. The nearly collinear signal-idler system generated by SPDC can be described by the two-photon state:

$$|\Psi\rangle = \Psi_0 \int d\vec{\kappa}_s d\vec{\kappa}_i \delta(\vec{\kappa}_s + \vec{\kappa}_i) \int d\omega_s d\omega_i \delta(\omega_s + \omega_i - \omega_p) a^\dagger(\vec{\kappa}_s, \omega_s) a^\dagger(\vec{\kappa}_i, \omega_i) |0\rangle \quad (11)$$

where  $\omega_j, \vec{\kappa}_j$  ( $j = s, i, p$ ), is the frequency and the transverse wavevector of the signal, idler, and pump. To simplify the calculation, we have assumed a CW single frequency plane-wave pump with  $\vec{\kappa}_p = 0$ . The joint-detection probability between the point-like detectors  $D_1$  and  $D_2$  located at  $(\vec{\rho}_1, z_1)$  and  $(\vec{\rho}_2, z_2)$ , respectively, is calculated from the Glauber theory of photodetection [11]:

$$\begin{aligned} G^{(2)}(\vec{\rho}_1, z_1, t_1; \vec{\rho}_2, z_2, t_2) &= |\langle 0 | E_2^{(+)}(\vec{\rho}_2, z_2, t_2) E_1^{(+)}(\vec{\rho}_1, z_1, t_1) | \Psi \rangle|^2 \\ &= |\Psi(\vec{\rho}_1, z_1, t_1; \vec{\rho}_2, z_2, t_2)|^2. \end{aligned} \quad (12)$$

At this point we are taking  $z_1 = z_2 = 0$ . The transverse part of the effective two-photon wavefunction  $\Psi(\vec{\rho}_1, \vec{\rho}_2)$  is thus calculated as:

$$\Psi(\vec{\rho}_1, \vec{\rho}_2) \simeq \Psi_0 \delta(\vec{\rho}_1 - \vec{\rho}_2). \quad (13)$$

Both Eqs. (11) and (13) suggest that the entangled signal-idler photon pair is characterized by EPR correlation [1] in transverse momentum and transverse position; hence, similar to the original EPR state, we have [7]:

$$\begin{aligned} \Delta(\vec{\kappa}_s + \vec{\kappa}_i) = 0 \quad \& \quad \Delta(\vec{\rho}_1 - \vec{\rho}_2) = 0 \\ \text{with } \Delta\vec{\kappa}_s \sim \infty, \quad \Delta\vec{\kappa}_i \sim \infty, \quad \Delta\vec{\rho}_1 \sim \infty, \quad \Delta\vec{\rho}_2 \sim \infty. \end{aligned} \quad (14)$$

In EPR's language, the signal and the idler may come out from any point on the output plane of the SPDC. However, if the signal (idler) is found in a certain position, the idler (signal) must be found in the same position, with certainty (100%). Furthermore, the signal and the idler may have any transverse momentum. However, if a certain value and direction of the transverse momentum of the signal (idler) is measured, the transverse momentum of the idler (signal) will certainly have equal value and opposite direction.

Concerning the experimental setup of Fig. 2, in light of Eq. (14), if the object is placed very close to the output plane of the SPDC crystal, the signal photon and the idler photon are guaranteed to come out from the same point of the object plane ( $\vec{\rho}_s = \vec{\rho}_i$ ) and to stop at the corresponding unique point on the image plane, thus forming an image together (i.e., a two-photon image), whether enlarged or demagnified. In addition, the signal-idler pair propagates in a special way in which the transverse momenta of the pair must satisfy  $\vec{\kappa}_s + \vec{\kappa}_i = 0$  and thus undergo "two-photon diffraction." Two-photon diffraction is radically different from that of two independent photons and yields a different spatial resolution of the image. This unique feature will be shown in the following calculation.

The fields at the detectors are the same as in the classical imaging case. By inserting the field operators into  $\Psi(\vec{\rho}_1, z_1, t_1; \vec{\rho}_2, z_2, t_2)$ , as defined in Eq. (12), and considering the commutation relations for the creation and the annihilation operators, we find for the effective two-photon

wavefunction in the image plane

$$\begin{aligned}
& \Psi(\vec{\rho}_1, z_1, t_1; \vec{\rho}_2, z_2, t_2) \\
= & \Psi_0 \int d\vec{\kappa}_s d\vec{\kappa}_i \delta(\vec{\kappa}_s + \vec{\kappa}_i) \int d\omega_s d\omega_i \delta(\omega_s + \omega_i - \omega_p) \\
& \times g(\vec{\kappa}_s, \omega_s; \vec{\rho}_1, z_1) e^{-i\omega_s t_1} g(\vec{\kappa}_i, \omega_i; \vec{\rho}_2, z_2) e^{-i\omega_i t_2}
\end{aligned} \tag{15}$$

Substituting the  $g$  functions of Eq. (7) into Eq. (15) and applying the  $\delta$ -functions in the state to reduce the variables of the integral in Eq. (15) from 4 to 2, we obtain

$$\begin{aligned}
& \Psi(\vec{\rho}_1, \tau_1; \vec{\rho}_2, \tau_2) \\
\propto & \int d\vec{\rho}'_o A(\vec{\rho}'_o) e^{i\frac{\omega_p}{2cs_o}|\vec{\rho}'_o|^2} \int d\vec{\rho}''_o A(\vec{\rho}''_o) e^{i\frac{\omega_p}{2cs_o}|\vec{\rho}''_o|^2} \\
& \times \int d\vec{\rho}_l e^{-i\frac{\omega_p}{2c}(\frac{\vec{\rho}_o}{s_o} + \frac{\vec{\rho}_l}{s_l}) \cdot \vec{\rho}_l} \int d\vec{\rho}'_l e^{-i\frac{\omega_p}{2c}(\frac{\vec{\rho}'_o}{s_o} + \frac{\vec{\rho}'_l}{s_l}) \cdot \vec{\rho}'_l} \\
& \times \left\{ \int d\nu e^{i\nu[(\tau_1 - \tau_2) + (\frac{\vec{\rho}_o}{cs_o} + \frac{\vec{\rho}_l}{cs_l}) \cdot \vec{\rho}_l - (\frac{\vec{\rho}'_o}{cs_o} + \frac{\vec{\rho}'_l}{cs_l}) \cdot \vec{\rho}'_l]} \right\} \\
& \times e^{-i\frac{\nu}{2cs_o}|\vec{\rho}_o|^2} e^{i\frac{\nu}{2cs_o}|\vec{\rho}'_o|^2} \left\{ \int d\vec{\kappa}_s e^{i\vec{\kappa}_s \cdot [\vec{\rho}_o - \vec{\rho}'_o]} \right\}
\end{aligned} \tag{16}$$

where  $\tau_j = t_j - z_j/c$ ,  $\nu$  is defined from  $\omega_s = \omega_p/2 + \nu$  and  $\omega_i = \omega_p/2 - \nu$  following  $\omega_s + \omega_i = \omega_p$ .

Now we consider a two-photon film (two-photon absorber), or equivalently scan  $D_1$  and  $D_2$  together, on the image plane to achieve  $\vec{\rho}_1 = \vec{\rho}_2$ ,  $z_1 = z_2$  and examine the two integrals in the two curly brackets. It is easy to see that the integral of  $d\vec{\kappa}_s$  yields  $\delta(\vec{\rho}_o - \vec{\rho}'_o)$ , which is consistent with Eq. (13). The integral of  $d\nu$  gives a similar  $\delta$ -function in the form of  $\delta[(\frac{\vec{\rho}_o}{cs_o} + \frac{\vec{\rho}_l}{cs_l})(\vec{\rho}_l - \vec{\rho}'_l)]$  while taking  $\vec{\rho}_o = \vec{\rho}'_o$ ,  $\vec{\rho}_1 = \vec{\rho}_2 = \vec{\rho}$ , and  $\tau_1 = \tau_2$ . These results indicate that the propagation-diffraction of the signal photon and the idler photon are not independent. The ‘‘two-photon diffraction’’ couples the two integrals in  $\vec{\rho}_o$  and  $\vec{\rho}'_o$  as well as the two integrals in  $\vec{\rho}_l$  and  $\vec{\rho}'_l$  and gives the  $G^{(2)}$  function

$$G^{(2)}(\vec{\rho}, \vec{\rho}) \propto \left| \int_{obj} d\vec{\rho}_o A^2(\vec{\rho}_o) e^{i\frac{\omega_p}{2cs_o}|\vec{\rho}_o|^2} \frac{2J_1\left(\frac{R}{s_o} \frac{\omega_p}{c} |\vec{\rho}_o + \frac{\vec{\rho}}{m}|\right)}{\left(\frac{R}{s_o} \frac{\omega_p}{c} |\vec{\rho}_o + \frac{\vec{\rho}}{m}|\right)^2} \right|^2 \tag{17}$$

which indicates that a coherent image magnified by a factor of  $m = s_i/s_o$  is reproduced on the image plane by joint-detection or by two-photon absorption.

In Eq. (17), the point-spread function is characterized by the pump wavelength  $\lambda_p = \lambda_{s,i}/2$ ; hence, the point-spread function is twice narrower than in the (first order) classical case. An entangled two-photon state thus gives an image in joint-detection with double spatial resolution when compared to what one would obtain in classical imaging. Moreover, the spatial resolution of the two-photon image obtained by SPDC is further improved because it is determined by the function  $2J_1(x)/x^2$ , which is much narrower than the  $somb(x)$ .

It is interesting to see that, different from the classical case, the frequency integral over  $\Delta\omega_s \sim \infty$  does not give any blurring problem, but rather enhances the spatial resolution of the two-photon image. These characteristics of entangled states may be useful for certain applications [24].

Can we replace entangled states with classical light in the same setup of Fig. 2 and still have a twice narrower point-spread function in two-photon joint-detection?

We will first quickly examine the case of coherent radiation. By definition, coherent light is characterized by the relation:  $G^{(2)} = |G^{(1)}|^2$  [11]. The two-photon image produced by laser



light is readily obtained from Eq. (10):

$$G^{(2)}(\vec{\rho}_1, \vec{\rho}_2) \propto \left| \int_{obj} d\vec{\rho}_o A(\vec{\rho}_o) e^{i\frac{\omega}{2cs_o}|\vec{\rho}_o|^2} \text{somb}\left[\frac{R}{s_o} \frac{\omega}{c} \left|\vec{\rho}_o + \frac{\vec{\rho}_1}{m}\right|\right] \right|^2 \times \left| \int_{obj} d\vec{\rho}_o A(\vec{\rho}_o) e^{i\frac{\omega}{2cs_o}|\vec{\rho}_o|^2} \text{somb}\left[\frac{R}{s_o} \frac{\omega}{c} \left|\vec{\rho}_o + \frac{\vec{\rho}_2}{m}\right|\right] \right|^2 \quad (18)$$

which is simply a product of two independent first-order coherent images (see Eq. (10)).

Now we analyze chaotic light. The standard form of the  $G^{(2)}$ -function of chaotic light is [16]:

$$G^{(2)}(\vec{\rho}_1, \vec{\rho}_2) = G_{11}^{(1)}(\vec{\rho}_1) G_{22}^{(1)}(\vec{\rho}_2) + |G_{12}^{(1)}(\vec{\rho}_1, \vec{\rho}_2)|^2, \quad (19)$$

where  $G_{11}^{(1)}(\vec{\rho}_1)$  and  $G_{22}^{(1)}(\vec{\rho}_2)$  are the mean intensity distributions on the image plane. It is straightforward to find that the first term of Eq. (19), i.e.,  $G_{11}^{(1)}(\vec{\rho}_1) G_{22}^{(1)}(\vec{\rho}_2)$ , is a simple product of two independent incoherent classical (first-order) images. The interesting part of Eq. (19) is in the second term where

$$G_{12}^{(1)}(\vec{\rho}_1, z_1, t_1; \vec{\rho}_2, z_2, t_2) \propto \int d\vec{k} g^*(\vec{k}, \omega; \vec{\rho}_1, z_1) e^{i\omega t_1} g(\vec{k}, \omega; \vec{\rho}_2, z_2) e^{-i\omega t_2}. \quad (20)$$

Substituting the  $g^*$  and  $g$  functions into Eq. (20) and considering  $D_1$  and  $D_2$  on the image plane, we obtain

$$G_{12}^{(1)}(\vec{\rho}_1, \vec{\rho}_2) \propto \int_{obj} d\vec{\rho}_o A^*(\vec{\rho}_o) e^{-i\frac{\omega}{2cs_o}|\vec{\rho}_o|^2} \int_{obj} d\vec{\rho}'_o A(\vec{\rho}'_o) e^{i\frac{\omega}{2cs_o}|\vec{\rho}'_o|^2} \times \int_{lens} d\vec{\rho}_l e^{i\frac{\omega}{c}(\frac{\vec{\rho}_o}{s_o} + \frac{\vec{\rho}_l}{s_i}) \cdot \vec{\rho}_l} \int_{lens} d\vec{\rho}'_l e^{-i\frac{\omega}{c}(\frac{\vec{\rho}'_o}{s_o} + \frac{\vec{\rho}'_l}{s_i}) \cdot \vec{\rho}'_l} \times \left\{ \int d\vec{k} e^{i\vec{k} \cdot [\vec{\rho}'_o - \vec{\rho}_o]} \right\}. \quad (21)$$

Similar to the first-order imaging, in Eqs. (20) and (21) we have assumed monochromatic light to avoid ‘‘aberration’’ complications. Differing from that of SPDC, here an integral of  $\Delta\omega \sim \infty$  results in a constant  $G_{12}^{(1)}$ , which is consistent with our experimental observation [17].

Evaluating the integrals in Eq. (21), the  $G_{12}^{(1)} G_{21}^{(1)}$  term turns out to be

$$|G_{12}^{(1)}(\vec{\rho}_1, \vec{\rho}_2)|^2 \propto \left| \int_{obj} d\vec{\rho}_o |A(\vec{\rho}_o)|^2 \text{somb}\left(\frac{R}{s_o} \frac{\omega}{c} \left|\vec{\rho}_o + \frac{\vec{\rho}_1}{m}\right|\right) \text{somb}\left(\frac{R}{s_o} \frac{\omega}{c} \left|\vec{\rho}_o + \frac{\vec{\rho}_2}{m}\right|\right) \right|^2. \quad (22)$$

Unlike the  $G_{11}^{(1)} G_{22}^{(1)}$  term, here, we do not have two independent images. This is the reason that chaotic light has been successfully used to mimic certain nonlocal features of entangled systems [18]. Chaotic light, however, is not a viable alternative to entangled sources for quantum lithography. In fact, when  $D_1$  and  $D_2$  are scanned together, or a two-photon sensitive material is employed for recording the photon pair, i.e.,  $\vec{\rho}_1 = \vec{\rho}_2 = \vec{\rho}$ , Eq. 22 becomes:

$$|G_{12}^{(1)}(\vec{\rho}, \vec{\rho})|^2 \propto \left| \int_{obj} d\vec{\rho}_o |A(\vec{\rho}_o)|^2 \left| \text{somb}\left[\frac{R}{s_o} \frac{\omega}{c} \left|\vec{\rho}_o + \frac{\vec{\rho}}{m}\right|\right] \right|^2 \right|^2 \quad (23)$$

which is the same result as given by the  $G_{11}^{(1)} G_{22}^{(1)}$  term. Namely, it is simply the product of two independent incoherent first-order classical images. This conclusion relates quite nicely to the findings of [25]: in that experiment, a doubly modulated interference-diffraction pattern was observed by scanning the detectors in opposite directions on the Fourier transform plane. However, no second-order interference pattern can be observed if the detectors are scanned together.

## 5 Ghost Imaging

Pittman *et al* demonstrated a surprising two-photon imaging experiment in 1995 [2]. The experiment was immediately named “ghost imaging” due to its “nonlocal” feature. The important physics demonstrated in the experiment, nevertheless, may not be the so called “ghost.” Indeed, the original purpose of the experiment was to study the EPR correlation in position and in momentum and to test the EPR inequality [4, 7, 6] for the entangled signal-idler photon pair of SPDC.

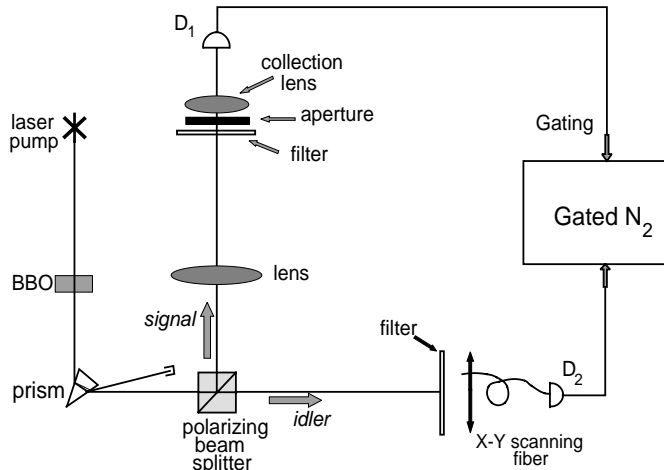


Figure 4: Schematic set-up of the “ghost” image experiment.

The schematic setup of the “ghost” imaging experiment is shown in Fig. 4. A CW laser is used to pump a nonlinear crystal, which is cut for degenerate type-II phase matching to produce a pair of orthogonally polarized signal (e-ray of the crystal) and idler (o-ray of the crystal) photon. The pair emerges from the crystal collinear, with  $\omega_s \cong \omega_i \cong \omega_p/2$ . The pump is then separated from the signal-idler pair by a dispersion prism, and the remaining signal and idler beams are sent in different directions by a polarization beam splitting Thompson prism. The signal beam passes through a convex lens with a  $400mm$  focal length and illuminates a chosen aperture (mask). As an example, one of the demonstrations used letters “UMBC” for the object mask. Behind the aperture is the “bucket” detector package  $D_1$ , which consists of a short focal length collection lens in whose focal spot is an avalanche photodiode.  $D_1$  is mounted in a fixed position during the experiment. The idler beam is met by detector package  $D_2$ , which consists of an optical fiber whose output is mated with another avalanche photodiode. The input tip of the fiber is scanned in the transverse plane by two step motors. The output pulses of each detector, which are operating in photon counting mode, are sent to a coincidence counting circuit for the signal-idler joint-detection.

By recording the coincidence counts as a function of the fiber tip’s transverse plane coordinates, the image of the chosen aperture (for example, “UMBC”) is observed, as reported in Fig. 5. It is interesting to note that while the size of the “UMBC” aperture inserted in the signal beam is only about  $3.5mm \times 7mm$ , the observed image measures  $7mm \times 14mm$ . The image is therefore magnified by a factor of 2. The observation also confirms that the focal length of the imaging lens  $f$ , the aperture’s optical distance from the lens  $S_o$ , and the image’s optical distance from the lens  $S_i$  (which is from the imaging lens going backward along the signal photon path to the two-photon source of SPDC crystal then going forward along the path of idler photon to the image), satisfy the Gaussian thin lens equation. In this experiment,  $S_o$  was chosen to be  $S_o = 600mm$ , and the twice magnified clear image was found when the fiber tip was on the plane of  $S_i = 1200mm$ . When  $D_2$  was scanned on transverse planes not determined by the Gaussian thin lens equation the images blurred out.

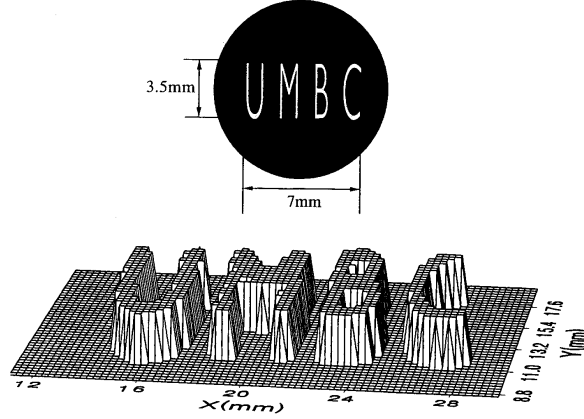


Figure 5: (a) A reproduction of the actual aperture “UMBC” placed in the signal beam. (b) The image of “UMBC”: coincidence counts as a function of the fiber tip’s transverse coordinates in the image plane. The step size is 0.25mm. The image shown is a “slice” at the half maximum value.

The measurement of the signal and the idler subsystem themselves are very different. The single photon counting rate of  $D_2$  was recorded during the scanning of the image and was found fairly constant in the entire region of the image. This means that the transverse coordinate uncertainty of either signal or idler is considerably large compared to that of the transverse correlation of the entangled signal-idler photon pair:  $\Delta x_1$  ( $\Delta y_1$ ) and  $\Delta x_2$  ( $\Delta y_2$ ) are much greater than  $\Delta(x_1 - x_2)$  ( $\Delta(y_1 - y_2)$ ).

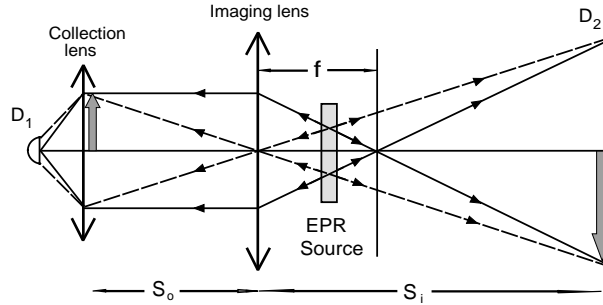


Figure 6: An unfolded setup of the ghost imaging experiment, which is helpful for understanding the physics. Since the two-photon “light” propagates along “straight-lines”, it is not difficult to find that any geometrical light point on the object plane corresponds to a unique geometrical light point on the image plane. Thus, a ghost image of the object is made nonlocally in the image plane. Although the placement of the lens, the object, and detector  $D_2$  obeys the Gaussian thin lens equation, it is important to remember that the geometric rays in the figure actually represent the two-photon amplitudes of an entangled photon pair. The point to point correspondence is the result of the superposition of these two-photon amplitudes.

The EPR  $\delta$ -functions,  $\delta(\vec{\rho}_s - \vec{\rho}_i)$  and  $\delta(\vec{\kappa}_s + \vec{\kappa}_i)$  in transverse dimension, are the key to understand this interesting phenomenon. In degenerate SPDC, although the signal-idler photon pair has equal probability to be emitted from any points on the output surface of the nonlinear crystal, the transverse position  $\delta$ -function indicates that if one of them is observed at one position, the other one must be found at the same position. In other words, the pair is always

emitted from the same point on the output plane of the two-photon source. Simultaneously, the transverse momentum  $\delta$ -function defines the angular correlation of the signal-idler pair. The transverse momenta of a signal-idler amplitude are always equal but pointed in opposite directions,  $\vec{\kappa}_s = -\vec{\kappa}_i$ , which means that the two-photon amplitudes are always existing at roughly equal yet opposite angles relative to the pump. This then allows for a simple explanation of the experiment in terms of “usual” geometrical optics in the following manner: we envision the nonlinear crystal as a “hinge point” and “unfold” the schematic of Fig. 4 into the Klyshko picture of Fig. 6. The signal-idler two-photon amplitudes can then be represented by straight lines (but keep in mind the different propagation directions) and therefore, the image is well produced in coincidences when the aperture, lens, and fiber tip are located according to the Gaussian thin lens equation of Eq. (2). The image is exactly the same as one would observe on a screen placed at the fiber tip if detector  $D_1$  were replaced by a point-like light source and the nonlinear crystal by a reflecting mirror.

Following a similar analysis in geometric optics, it is not difficult to find that any geometrical “light spot” on the object plane, which is the intersection point of all possible two-photon amplitudes coming from the two-photon light source, corresponds to an unique geometrical “light spot” on the image plane, which is another intersection point of all the possible two-photon amplitudes. This point to point correspondence made the “ghost” image of the subject-aperture possible. Despite the completely different physics from classical geometrical optics, the remarkable feature is that the relationship between the focal length of the lens  $f$ , the aperture’s optical distance from the lens  $S_o$ , and the image’s optical distance from the lens  $S_i$ , satisfy the Gaussian thin lens equation of Eq. (2). Although the placement of the lens, the object, and the detector  $D_2$  obeys the Gaussian thin lens equation, it is important to remember that the geometric rays in the figure actually represent the two-photon amplitudes of a signal-idler photon pair and the point to point correspondence is the result of the superposition of these two-photon amplitudes. The “ghost” image is a realization of the 1935 EPR *gedankenexperiment*.

Now we calculate  $G^{(2)}(\vec{\rho}_o, \vec{\rho}_i)$  for the “ghost” imaging experiment, where  $\vec{\rho}_o$  and  $\vec{\rho}_i$  are the transverse coordinates on the object plane and the image plane. We will show that there exists a  $\delta$ -function like point-to-point correlation between the object plane and the image plane, i.e., if one measures the signal photon at a position of  $\vec{\rho}_o$  on the object plane the idler photon can be found only at a certain unique position of  $\vec{\rho}_i$  on the image plane satisfying  $\delta(\vec{\rho}_o - \vec{\rho}_i/m)$ , where  $m = -(s_i/s_o)$  is the image-object magnification factor. After approving the  $\delta$ -function correlation, we show how the object function of  $A(\vec{\rho}_o)$  is transferred to the image plane as a magnified image  $A(\vec{\rho}_i/m)$ . Before starting the calculation, it is worth to emphasize again that the “straight lines” in Fig. 6 schematically represent the two-photon amplitudes all belong to a pair of signal-idler photon. A “click-click” joint measurement at  $(\mathbf{r}_1, t_1)$ , which is on the object plane, and  $(\mathbf{r}_2, t_2)$ , which is on the image plane, in the form of EPR  $\delta$ -function, is the result of the coherent superposition of all these two-photon amplitudes.

We follow the unfolded experimental setup shown in Fig. 7 to establish the Green’s functions  $g(\vec{\kappa}_s, \omega_s, \vec{\rho}_o, z_o)$  and  $g(\vec{\kappa}_i, \omega_i, \vec{\rho}_2, z_2)$ . In arm-1, the signal propagates freely over a distance  $d_1$  from the output plane of the source to the imaging lens, then passes an object aperture at distance  $s_o$ , and then is focused onto photon counting detector  $D_1$  by a collection lens. We will evaluate  $g(\vec{\kappa}_s, \omega_s, \vec{\rho}_o, z_o)$  by propagating the field from the output plane of the two-photon source to the object plane. In arm-2, the idler propagates freely over a distance  $d_2$  from the output plane of the two-photon source to a point-like detector  $D_2$ .  $g(\vec{\kappa}_i, \omega_i, \vec{\rho}_2, z_2)$  is thus a free propagator.

(I) Arm-1 (source to object):

The optical transfer function or Green’s function in arm-1, which propagates the field from

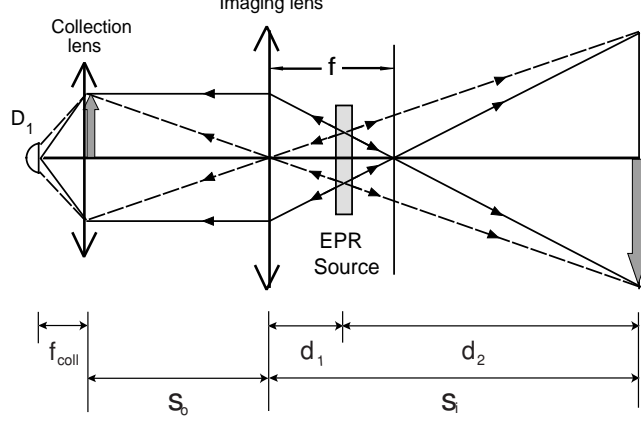


Figure 7: In arm-1, the signal propagates freely over a distance  $d_1$  from the output plane of the source to the imaging lens, then passes an object aperture at distance  $s_o$ , and then is focused onto photon counting detector  $D_1$  by a collection lens. In arm-2, the idler propagates freely over a distance  $d_2$  from the output plane of the source to a point-like photon counting detector  $D_2$ .

the source plane to the object plane, is given by:

$$\begin{aligned}
& g(\vec{\kappa}_s, \omega_s; \vec{\rho}_o, z_o = d_1 + s_o) \\
&= e^{i\frac{\omega_s}{c}z_o} \int_{lens} d\vec{\rho}_l \int_{source} d\vec{\rho}_s \left\{ \frac{-i\omega_s}{2\pi c d_1} e^{i\vec{\kappa}_s \cdot \vec{\rho}_s} e^{i\frac{\omega_s}{2c d_1} |\vec{\rho}_s - \vec{\rho}_l|^2} \right\} \\
&\quad \times e^{-i\frac{\omega_s}{2c f} |\vec{\rho}_l|^2} \left\{ \frac{-i\omega_s}{2\pi c s_o} e^{i\frac{\omega_s}{2c s_o} |\vec{\rho}_l - \vec{\rho}_o|^2} \right\}, \tag{24}
\end{aligned}$$

where  $\vec{\rho}_s$  and  $\vec{\rho}_l$  are the transverse vectors defined, respectively, on the output plane of the source and on the plane of the imaging lens. The terms in the first and second curly brackets in Eq. (24) describe free space propagation from the output plane of the source to the imaging lens and from the imaging lens to the object plane, respectively. Again,  $e^{i\frac{\omega_s}{2c d_1} |\vec{\rho}_s - \vec{\rho}_l|^2}$  and  $e^{i\frac{\omega_s}{2c s_o} |\vec{\rho}_l - \vec{\rho}_o|^2}$  are the Fresnel phases we have defined in Appendix A. Here, we treat the imaging lens as a thin-lens. Thus, the transformation function of the imaging lens is approximated as a Gaussian  $l(|\vec{\rho}_l|, f) \cong e^{-i\frac{\omega_s}{2c f} |\vec{\rho}_l|^2}$ .

(II) Arm-2 (from source to image):

In arm-2, the idler propagates freely from the source to the plane of  $D_2$ , which is also the plane of the image. The Green's function is thus:

$$g(\vec{\kappa}_i, \omega_i; \vec{\rho}_2, z_2 = d_2) = \frac{-i\omega_i}{2\pi c d_2} e^{i\frac{\omega_i}{c} d_2} \int_{source} d\vec{\rho}'_s e^{i\frac{\omega_i}{2c d_2} |\vec{\rho}'_s - \vec{\rho}_2|^2} e^{i\vec{\kappa}_i \cdot \vec{\rho}'_s} \tag{25}$$

where  $\vec{\rho}'_s$  and  $\vec{\rho}_2$  are the transverse vectors defined, respectively, on the output plane of the source, and on the plane of the photodetector  $D_2$ .

(III)  $\Psi(\vec{\rho}_o, \vec{\rho}_i)$  and  $G^{(2)}(\vec{\rho}_o, \vec{\rho}_i)$  (object plane - image plane):

To simplify the calculation and to focus on the transverse correlation, in the following calculation we assume degenerate ( $\omega_s = \omega_i = \omega$ ) and collinear SPDC. The transverse two-photon effective wavefunction  $\Psi(\vec{\rho}_o, \vec{\rho}_2)$  is then evaluated by substituting the Green's functions

$g(\vec{\kappa}_s, \omega; \vec{\rho}_o, z_o)$  and  $g(\vec{\kappa}_i, \omega; \vec{\rho}_2, z_2)$  into the expression given in Eq. (15):

$$\begin{aligned}
\Psi(\vec{\rho}_o, \vec{\rho}_2) &\propto \int d\vec{\kappa}_s d\vec{\kappa}_i \delta(\vec{\kappa}_s + \vec{\kappa}_i) g(\vec{\kappa}_s, \omega; \vec{\rho}_o, z_o) g(\vec{\kappa}_i, \omega; \vec{\rho}_2, z_2) \\
&\propto e^{i\frac{\omega}{c}(s_o+s_i)} \int d\vec{\kappa}_s d\vec{\kappa}_i \delta(\vec{\kappa}_s + \vec{\kappa}_i) \\
&\times \int_{lens} d\vec{\rho}_l \int_{source} d\vec{\rho}_s e^{i\vec{\kappa}_s \cdot \vec{\rho}_s} e^{i\frac{\omega}{2cd_1}|\vec{\rho}_s - \vec{\rho}_l|^2} \\
&\quad \times e^{-i\frac{\omega}{2cf}|\vec{\rho}_l|^2} e^{i\frac{\omega}{2cs_o}|\vec{\rho}_l - \vec{\rho}_o|^2} \\
&\times \int_{source} d\vec{\rho}'_s e^{i\vec{\kappa}_i \cdot \vec{\rho}'_s} e^{i\frac{\omega}{2cd_2}|\vec{\rho}'_s - \vec{\rho}_2|^2}
\end{aligned} \tag{26}$$

where we have ignored all the proportional constants. Completing the double integral of  $d\vec{\kappa}_s$  and  $d\vec{\kappa}_i$

$$\int d\vec{\kappa}_s d\vec{\kappa}_i \delta(\vec{\kappa}_s + \vec{\kappa}_i) e^{i\vec{\kappa}_s \cdot \vec{\rho}_s} e^{i\vec{\kappa}_i \cdot \vec{\rho}'_s} \sim \delta(\vec{\rho}_s - \vec{\rho}'_s), \tag{27}$$

Eq. (26) becomes:

$$\begin{aligned}
\Psi(\vec{\rho}_o, \vec{\rho}_2) &\tag{28} \\
\propto e^{i\frac{\omega}{c}(s_o+s_i)} \int_{lens} d\vec{\rho}_l \int_{source} d\vec{\rho}_s e^{i\frac{\omega}{2cd_2}|\vec{\rho}_2 - \vec{\rho}_s|^2} e^{i\frac{\omega}{2cd_1}|\vec{\rho}_s - \vec{\rho}_l|^2} e^{-i\frac{\omega}{2cf}|\vec{\rho}_l|^2} e^{i\frac{\omega}{2cs_o}|\vec{\rho}_l - \vec{\rho}_o|^2}.
\end{aligned}$$

We then complete the integral on  $d\vec{\rho}_s$ ,

$$\Psi(\vec{\rho}_o, \vec{\rho}_2) \propto e^{i\frac{\omega}{c}(s_o+s_i)} \int_{lens} d\vec{\rho}_l e^{i\frac{\omega}{2cs_i}|\vec{\rho}_2 - \vec{\rho}_l|^2} e^{-i\frac{\omega}{2cf}|\vec{\rho}_l|^2} e^{i\frac{\omega}{2cs_o}|\vec{\rho}_l - \vec{\rho}_o|^2}, \tag{29}$$

where we have replaced  $d_1 + d_2$  with  $s_i$  (as depicted in Fig. 7). Although the signal and idler propagate to different directions along two optical arms, Interestingly, the Green function in Eq. (29) is equivalent to that of a classical imaging setup, if we imagine the fields start propagating from a point  $\vec{\rho}_o$  on the object plane to the lens and then stop at point  $\vec{\rho}_2$  on the imaging plane ( $\vec{\rho}_2 = \vec{\rho}_i$ ). The mathematics is consistent with our previous qualitative analysis of the experiment.

The integral on  $d\vec{\rho}_l$  yields a point-to-point relationship between the object plane and the image plane that is defined by the Gaussian thin-lens equation:

$$\int_{lens} d\vec{\rho}_l e^{i\frac{\omega}{2c}[\frac{1}{s_o} + \frac{1}{s_i} - \frac{1}{f}]|\vec{\rho}_l|^2} e^{-i\frac{\omega}{c}(\frac{\vec{\rho}_o}{s_o} + \frac{\vec{\rho}_i}{s_i}) \cdot \vec{\rho}_l} \sim \delta(\vec{\rho}_o + \vec{\rho}_i/m), \tag{30}$$

where we have replaced  $\vec{\rho}_2$  with  $\vec{\rho}_i$ . In Eq. (30), the integral is approximated to infinity and the Gaussian thin-lens equation of Eq (2) is applied. We have also defined  $m = s_i/s_o$  as the magnification factor of the imaging system. The function  $\delta(\vec{\rho}_o + \vec{\rho}_i/m)$  indicates that a point of  $\vec{\rho}_o$  on the object plane corresponds to a unique point of  $\vec{\rho}_i$  on the image plane. The two vectors pointed to opposite directions and the magnitudes of the two vectors hold a ratio of  $m = |\vec{\rho}_i|/|\vec{\rho}_o|$ .

If the finite size of the imaging lens has to be taken into account (finite radius  $R$ ), the integral yields a point-spread function of  $somb(x)$ :

$$\int_{lens} d\vec{\rho}_l e^{-i\frac{\omega}{c}(\frac{\vec{\rho}_o}{s_o} + \frac{\vec{\rho}_i}{s_i}) \cdot \vec{\rho}_l} \propto somb\left(\frac{R}{s_o} \frac{\omega}{c} [\vec{\rho}_o + \frac{\vec{\rho}_i}{m}]\right) \tag{31}$$

where, again,  $somb(x) = 2J_1(x)/x$ ,  $J_1(x)$  is the first-order Bessel function. The point-spread function turns the point-to-point correspondence between the object plane and the image plane into a point-to-“spot” relationship and thus limits the spatial resolution.

Therefore, by imposing the condition of the Gaussian thin-lens equation, the transverse two-photon effective wavefunction is approximated as a  $\delta$  function

$$\Psi(\vec{\rho}_o, \vec{\rho}_i) \sim \delta(\vec{\rho}_o + \vec{\rho}_i/m), \quad (32)$$

which indicates a point to point EPR correlation between the object plane and the image plane, i.e., if one observes the signal photon at a position of  $\vec{\rho}_o$  on the object plane, the idler photon can only be found at a certain unique position of  $\vec{\rho}_i$  on the image plane satisfying  $\vec{\rho}_o + \vec{\rho}_i/m = 0$  with  $m = s_i/s_o$ .

We now include an object-aperture function, a collection lens and a photon counting detector  $D_1$  into the optical transfer function of arm-1 as shown in Fig. 4. The collection-lens- $D_1$  package can be simply treated as a “bucket” detector. The “bucket” detector integrates all  $\Psi(\vec{\rho}_o, \vec{\rho}_2)$  that pass the object aperture  $A(\vec{\rho}_o)$  as a joint photodetection event. This process is equivalent to the following convolution:

$$R_{1,2} \propto \int_{object} d\vec{\rho}_o |A(\vec{\rho}_o)|^2 |\Psi(\vec{\rho}_o, \vec{\rho}_i)|^2 \simeq |A(\vec{\rho}_i/m)|^2 \quad (33)$$

where, again,  $D_2$  is scanning in the image plane,  $\vec{\rho}_2 = \vec{\rho}_i$ .

As we have discussed earlier, the position-position EPR correlation is the result of the coherent superposition of two-photon amplitudes.

$$G^{(2)}(\vec{\rho}_o, \vec{\rho}_i) = \left| \int d\vec{\kappa}_s d\vec{\kappa}_i \delta(\vec{\kappa}_s + \vec{\kappa}_i) g(\vec{\kappa}_s, \vec{\rho}_o) g(\vec{\kappa}_i, \vec{\rho}_2) \right|^2 \quad (34)$$

In principle, one signal-idler pair contains all the necessary two-photon amplitudes that generate the point-to-point correspondence between the object and the ghost image plane. To emphasize this concept, we name this kind of ghost image as *two-photon coherent* image.

We emphasize again, one should not confuse a classical “momentum-momentum” correlation with the EPR correlation in position and in momentum. Figure 8 is a schematic picture of the experiment of Bennink *et al.* [12], which distinguishes a trivial classical momentum-momentum correlation from EPR.

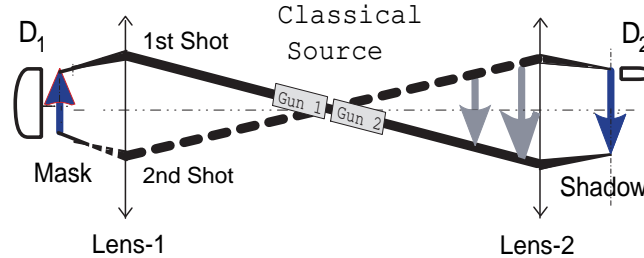


Figure 8: The projection shadow of an object mask is reproduced in coincidences between  $D_1$  and  $D_2$  by the use of two co-rotating correlated laser beams. The object-shadow correspondence is an accumulation of the “momentum-momentum” correlation between each pair of “shots”.

## 6 Ghost Imaging of Chaotic Light

Unlike first-order correlation, which is considered as a coherent effect of the electromagnetic field, the second-order correlation of radiation is usually considered as the statistical correlation

of intensity fluctuations. The first set of second-order correlation of thermal light was demonstrated in 1956 by Hanbury Brown and Twiss (HBT) with two different type of correlations: temporal and spatial [16]. The HBT experiment created quite a surprise in the physics community with an enduring debate about the classical or quantum nature of the phenomenon. It has been popular to consider that the HBT experiment measures the classical statistical correlation of the intensity fluctuations of the radiation [26]:

$$\langle \Delta I_1 \Delta I_2 \rangle = \langle (I_1 - \bar{I}_1)(I_2 - \bar{I}_2) \rangle = \langle I_1 I_2 \rangle - \bar{I}_1 \bar{I}_2 \quad (35)$$

where  $\bar{I}_1$  and  $\bar{I}_2$  are the mean intensities of the radiation measured by photodetectors  $D_1$  and  $D_2$ , respectively.

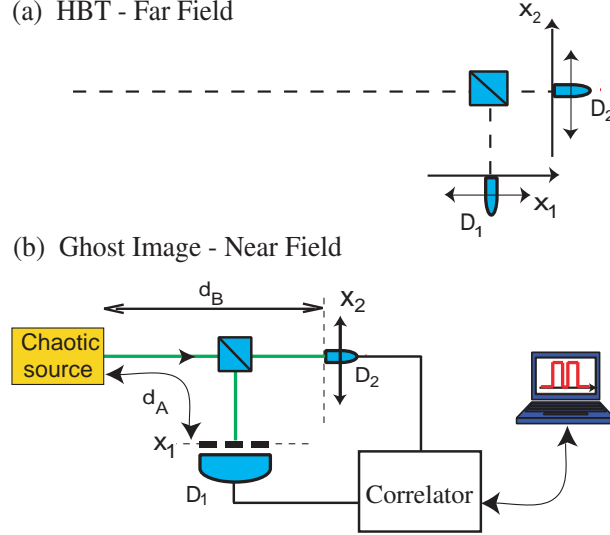


Figure 9: (a) Hanbury Brown and Twiss configuration. (b) lens-less Ghost imaging configuration.

Figure 9 (a) is a schematic of the historical HBT experiment which measures the second-order transverse spatial correlation of a monochromatic radiation of wavelength  $\lambda$  coming from a distant star with an angular size of  $\Delta\theta$ . Both photodetectors  $D_1$  and  $D_2$  can be scanned along the axes  $x_1$  and  $x_2$ , here, we assume 1-D scanning to simplify the discussion. The second-order transverse spatial correlation function  $\Gamma^{(2)}(x_1, x_2)$  is expected to be

$$\Gamma^{(2)}(x_1, x_2) = \langle I_1 I_2 \rangle \sim I_0^2 \left\{ 1 + \text{sinc}^2 \left[ \frac{\pi \Delta\theta (x_1 + x_2)}{\lambda} \right] \right\} \quad (36)$$

where we have simplified the problem to 1-D and assumed  $\bar{I}_1 = \bar{I}_2 = I_0$ . The second term in Eq. (36),  $I_0^2 \text{sinc}^2[\pi \Delta\theta (x_1 + x_2)/\lambda]$ , is interpreted as the correlation of intensity fluctuations. This term is useful in astronomy for angular size measurement of stars. For short wavelengths, this function quickly drops from its maximum to minimum when  $x_1 + x_2$  goes from zero to a value such that  $\Delta\theta (x_1 + x_2)/\lambda = 1$ . Thus, we effectively have a “point” to “point” relationship between the  $x_1$  and  $x_2$  plane, i.e., for each positive (negative) value of  $x_1$  there exist only one negative (positive) value of  $x_2$  that may have nonzero correlation of intensity fluctuation. In fact, the planes of  $x_1$  and  $x_2$  are in the far-field zone of the finite-size distant star (equivalent to the Fourier transform plane). Therefore, the measured quantity is the correlation between the transverse  $\mathbf{k}$  vectors of the radiation. For a narrow function, the non-zero correlation corresponds to the case of equal transverse wavevectors:  $\vec{\kappa}_1 = \vec{\kappa}_2$ . This is consistent with the physics behind the model of classical correlation. It is natural to imagine that the radiation coming from the same mode of the electromagnetic field, passing through the same optical



path, would have identical intensity fluctuations, while radiation coming from different modes, passing through different optical paths would not share the same intensity fluctuations.

Quantum models of HBT experiment derives the same correlation function [27][28]. However, if “classical” works, why quantum? The classical statistical interpretation has been widely accepted. Moreover, the concept of intensity fluctuation correlation has been even extended to quantum models to take over the concept of two-photon coherence. The philosophy of “photon bunching” is essentially a phenomenological extension to quantum theory of the statistical correlation on photon number fluctuations.

In the past twenty years, the massive research on quantum entanglement has brought new challenges to the classical statistical correlation interpretation. For example, replacing the chaotic light with an EPR type two-photon entangled state in Fig. 9 (a), the second-order transverse spatial correlation function turns out to be

$$\langle I_1 I_2 \rangle \sim I_0^2 \text{sinc}^2 \left[ \frac{\pi \Delta \theta (x_1 - x_2)}{\lambda} \right]. \quad (37)$$

Based on the concept of classical statistical correlation of intensity fluctuation, the mean intensities  $\bar{I}_1$  and  $\bar{I}_2$  must be zero in this case, otherwise Eq. (35) leads to non-physical conclusions. The measurements, however, never yield zero mean values of  $\bar{I}_1$  and  $\bar{I}_2$  in any circumstances.

Thus the concept of classical statistical correlation of intensity fluctuation may not work for entangled two-photon states. Two-photon correlation experiments with entangled photons have been explained in terms of the superposition of indistinguishable alternatives, i.e., two-photon probability amplitudes, that can lead to a joint-detection event [4]. Such alternatives, however, represent a troubling concept in classical theories, because this concept has no counterpart in classical electromagnetic theory of light and it is nonlocal. If accepted, the nonlocal behavior of the radiation has been classified as a peculiar property of non-classical sources.

More interestingly, we further ask ourselves: does the statistical correlation of intensity fluctuation always work for chaotic light? We are going to analyze a recent ghost imaging experiment of chaotic light by Scarcelli *et al.*, aimed at answering this question: “Can two-photon correlation of chaotic light be considered as correlation of intensity fluctuations?” [18] We will conclude that the second-order correlation of chaotic light is a *two-photon interference* phenomenon.

Figure 9 (b) illustrates the setup of the experiment. Radiation from a chaotic pseudothermal source [29] was divided in two optical paths by a non-polarizing beam splitter. In arm *A* an object, a double slit with slit separation  $d = 1.5\text{mm}$  and slit width  $a = 0.2\text{mm}$ , was placed at a distance  $d_A = 139\text{mm}$  and a bucket detector ( $D_1$ ) was just behind the object. In arm *B* a point detector  $D_2$  scanned the transverse planes in the neighborhood of a distance  $d_B = d_A$  from the source. The correlation was measured by either photon-counting-coincidence circuit or by standard HBT correlator. In the photon counting regime, two Geiger mode avalanche photodiodes were employed for single-photon level measurement. In HBT scheme, the two photodetectors were Silicon PIN photodiodes. The bucket detector  $D_1$  was simulated by using a short focal length lens ( $f = 25\text{mm}$ ) to focus the light onto the active area of the detector while the point detector  $D_2$  was simulated by a pinhole.

Figure 10 reports the measured two-photon image of the double-slit. The result shows an equal-size reproduction of the double slit when scanning photodetector  $D_2$  along  $x_2$  axis, which is located at distance  $d_B = d_A$  from the source. In Fig. 10, the DC background is subtracted from the image. Here, again, we have made a 1-D scanning to simplify the discussion.

Let us first clarify the main differences of this measurement compared to Hanbury Brown and Twiss types of experiments. As we described in the beginning of this section, the measurements of HBT are in the *far-field* zone, which measure the *momentum-momentum* correlation of the field. In the reported experiment, instead, the measurements were in the *near field* zone ( $\Delta \theta \sim 10\lambda/d$ ) and therefore effectively measured the *position-position* correlation between the object plane and the image plane. The observation is a lensless two-photon ghost image.

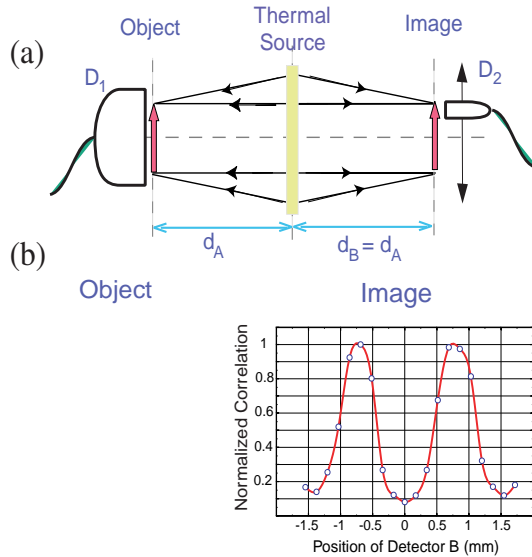


Figure 10: The results of Lensless imaging. Normalized two-photon correlation vs transverse position of  $D_2$ . The DC constant is subtracted from the correlation.

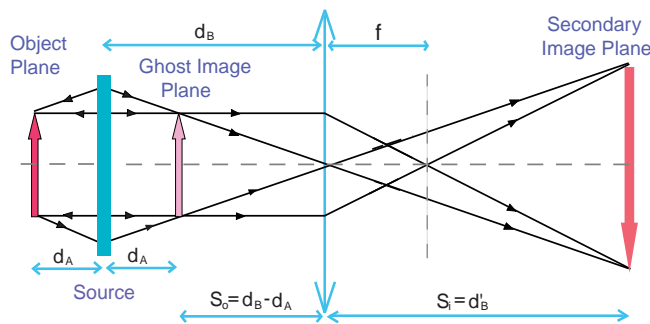


Figure 11: Schematic experimental setup of a secondary image measurement.

To confirm that the observed results corresponded to an image, Scarcelli *et al.* constructed a secondary imaging system, which is illustrated in Fig. 11, by using a  $f = 85\text{mm}$  lens to image the ghost image onto a secondary image plane. The imaging lens was located at a distance of  $d_B \sim 253\text{mm}$  from the source. A magnified secondary image was observed at  $d'_B \sim 330\text{mm}$  from the lens, which is given by the Gaussian thin lens equation, by scanning  $D_2$  on the transverse plane. Fig. 12 reports the measured magnified secondary image of the ghost image with the expected magnification  $M = d'_B / (d_B - d_A) \sim 2.9$ . For this examination this experiment used two masks with more complicated structures: one, Fig. 12(a), with the starting letter of the cities of the authors ( $2.3 \times 2.5 \text{ mm}$ ) and the other, Fig. 12(b), with the acronym of their institution ( $6 \times 1.9 \text{ mm}$ ). Fig. 12(c) shows the image obtained with the actual revealed correlation measurements to show the high contrast of the image, while in Fig. 12(d) is shown a “slice” of the image around the half maximum of the correlation.

The lens-less ghost imaging setup of Scarcelli *et al.* is a straightforward modification of the HBT. One needs simply move the two HBT photodetector from far-field to near-field. We cannot stop to ask: What has been preventing this simple move for 50 years (1956-2006)? Something must be terribly misleading to give us such misled confidence not even to try the near-field measurement in half a century.

The classical model in terms of statistical correlation of intensity fluctuations would not work for Scarcelli’s experiment. Unlike the HBT experiment in which the correlation was mea-

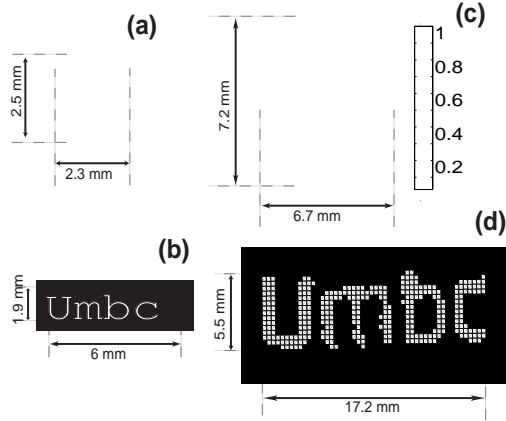


Figure 12: Results of the secondary Imaging. On the left, (a) and (b) are the two object used, on the right are shown the obtained images: (c) is a density plot of the normalized correlation, (d) is a “slice” of the measured correlation around the half maximum.

sured in the far-field zone. Scarcelli’s experiment is in near-field. In the near-field configuration, any point on the object plane and on the image plane are “hit” by many different  $\mathbf{k}$  vectors (modes). Fig. 13 schematically illustrates the situation. Assuming a chaotic radiation source of finite dimension consists of a large number of  $N$  point sub-sources. By definition of “chaotic”, each point sub-sources radiate and fluctuate independently and randomly. Now, we place two point photodetectors in near-field as illustrated in Fig. 13 and make a similar correlation measurement as that of HBT. It is easy to see that the chance of receiving radiation from the same sub-source is less then that of receiving from different sub-sources. The ratio between the two cases is approximately  $N/N^2$ . For a large number of  $N$ , the contributions from “identical sub-source” is negligible and thus  $\langle \Delta I_1 \Delta I_2 \rangle = 0$ , as we know that different sub-sources of chaotic light fluctuate randomly and independently. HBT is a special case. The two photodetectors are placed in far-field. A far-field plane is equivalent to the Fourier transform plane. On the Fourier transform plane, each point corresponds to a mode of radiation, and corresponds to a point sub-source. Thus, the chance for the two photodetectors to receive “identical mode”, or receive radiations from “identical point sub-sources”, is non-negligible. In this situation,  $\langle \Delta I_1 \Delta I_2 \rangle \neq 0$ .

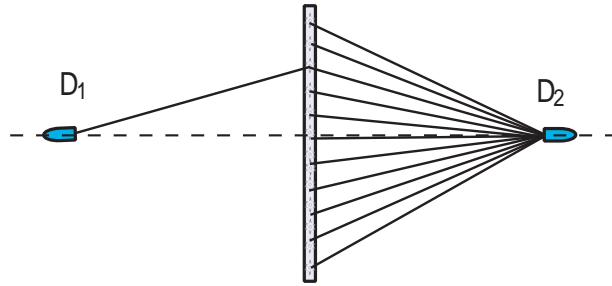


Figure 13: A simplified model of near-field joint detection of chaotic source. It is easy to see that the chance of receiving radiation from the same sub-source is less then that of receiving from different sub-sources.

On the other hand, the quantum model for Scarcelli’s experiment is straightforward. Even if the source is a “classical” chaotic light, the ghost image is explained as a quantum two-photon

effect. In a joint photodetection event of chaotic radiation, due to the superposition of two-photon amplitudes, there exists 50% chance for a precise position-position correlation, i.e., if photon 1 is measured at  $\vec{\rho}_1$ , photon two can only be measured at a unique certain position of  $\vec{\rho}_2$ . The following is a brief quantum mechanical calculation for the second-order correlation of chaotic radiation.

In the quantum theory of photodetection [11], the second-order correlation function is given in Eq. (12). What we need to do now is to find the state of the radiation and the operators of the field. In the *photon counting* regime, it is reasonable to model the thermal light in terms of *single photon states*. We have provided a simple model of thermal state in Appendix B. Similar to our earlier discussion, we will focus on the transverse correlation and assume the thermal radiation monochromatic:

$$\hat{\rho} \simeq |0\rangle\langle 0| + |\epsilon|^4 \sum_{\vec{\kappa}} \sum_{\vec{\kappa}'} \hat{a}^\dagger(\vec{\kappa}) \hat{a}^\dagger(\vec{\kappa}') |0\rangle\langle 0| \hat{a}(\vec{\kappa}') \hat{a}(\vec{\kappa}) \quad (38)$$

where  $|\epsilon| \ll 1$ . Basically we are modeling the light source as an incoherent statistical mixture of two photons with equal probability of having any transverse momentum  $\vec{\kappa}$  and  $\vec{\kappa}'$ .

The transverse spatial part of the second order correlation function is thus:

$$\begin{aligned} G^{(2)}(\vec{\rho}_1; \vec{\rho}_2) &= \sum_{\vec{\kappa}, \vec{\kappa}'} \langle 1_{\vec{\kappa}} 1_{\vec{\kappa}'} | E_1^{(-)}(\vec{\rho}_1) E_2^{(-)}(\vec{\rho}_2) E_2^{(+)}(\vec{\rho}_2) E_1^{(+)}(\vec{\rho}_1) | 1_{\vec{\kappa}} 1_{\vec{\kappa}'} \rangle \\ &= \sum_{\vec{\kappa}, \vec{\kappa}'} |\langle 0 | E_2^{(+)}(\vec{\rho}_2) E_1^{(+)}(\vec{\rho}_1) | 1_{\vec{\kappa}} 1_{\vec{\kappa}'} \rangle|^2. \end{aligned} \quad (39)$$

where  $\vec{\rho}_j$  is the transverse coordinate of the  $j^{\text{th}}$  detector. The transverse part of the electric field operator can be written as follows:

$$E_j^{(+)}(\vec{\rho}_j) \propto \sum_{\vec{\kappa}} g_j(\vec{\rho}_j; \vec{\kappa}) \hat{a}(\vec{\kappa}) \quad (40)$$

where  $\hat{a}(\vec{\kappa})$  is the annihilation operator for the mode corresponding to  $\vec{\kappa}$  and  $g_j(\vec{\rho}_j; \vec{\kappa})$  is the Green's function associated to the propagation of the field from the source to the  $j^{\text{th}}$  detector [21].

Substituting the field operators into Eq. (39) we obtain:

$$G^{(2)}(\vec{\rho}_1; \vec{\rho}_2) = \sum_{\vec{\kappa}, \vec{\kappa}'} |g_2(\vec{\rho}_2, \vec{\kappa}) g_1(\vec{\rho}_1, \vec{\kappa}') + g_2(\vec{\rho}_2, \vec{\kappa}') g_1(\vec{\rho}_1, \vec{\kappa})|^2. \quad (41)$$

This expression represents the key result toward the understanding of the phenomenon. In fact, it expresses an interference between two alternatives, different yet equivalent, which lead to a joint photodetection. The interference phenomenon is not, as in classical optics, due to the superposition of electromagnetic fields at a local point of space-time. It is due to the superposition of  $g_2(\vec{\rho}_2, \vec{\kappa}) g_1(\vec{\rho}_1, \vec{\kappa}')$  and  $g_2(\vec{\rho}_2, \vec{\kappa}') g_1(\vec{\rho}_1, \vec{\kappa})$ , the so-called two-photon amplitudes, non-classical entities that involve both arms of the optical setup as well as two distant photodetection events. Eq. (41) can be further evaluated into the form of

$$\begin{aligned} G^{(2)}(\vec{\rho}_1; \vec{\rho}_2) &\propto \sum_{\vec{\kappa}} |g_1(\vec{\rho}_1, \vec{\kappa})|^2 \sum_{\vec{\kappa}'} |g_2(\vec{\rho}_2, \vec{\kappa}')|^2 + \left| \sum_{\vec{\kappa}} g_1^*(\vec{\rho}_1, \vec{\kappa}) g_2(\vec{\rho}_2, \vec{\kappa}) \right|^2 \\ &= G_{11}^{(1)}(\vec{\rho}_1) G_{22}^{(1)}(\vec{\rho}_2) + |G_{12}^{(1)}(\vec{\rho}_1; \vec{\rho}_2)|^2. \end{aligned} \quad (42)$$

In Eq. (42), we have linked  $G^{(2)}$  with the first order correlation functions of  $G_{ij}^{(1)}$ . The first term in Eq. (42) is the product of the mean intensities measured by the two detectors. The second term, which corresponds to the ‘‘intensity fluctuation correlation’’ in Eq. (35), is nothing but the two-photon interference term. The superposition takes place between quantities  $g_2(\vec{\rho}_2, \vec{\kappa}) g_1(\vec{\rho}_1, \vec{\kappa}')$  and  $g_2(\vec{\rho}_2, \vec{\kappa}') g_1(\vec{\rho}_1, \vec{\kappa})$  in Eq. (41), namely the two-photon amplitudes.

Now, we calculate the  $|G_{12}^{(1)}(\vec{\rho}_1; \vec{\rho}_2)|^2$  term of Eq. (42). Following the experimental setup of Fig. 9 (b), the Green's function of free-propagation can be written as:

$$g_1(\vec{\rho}_1; \vec{\kappa}) = \int d\vec{\rho}_s \left\{ \frac{-i\omega}{2\pi c} \frac{e^{i\frac{\omega}{c}d_A}}{d_A} e^{i\frac{\omega}{2cd_A}|\vec{\rho}_1 - \vec{\rho}_s|^2} \right\} e^{-i\vec{\kappa} \cdot \vec{\rho}_s}$$

$$g_2(\vec{\rho}_2; \vec{\kappa}) = \int d\vec{\rho}_s \left\{ \frac{-i\omega}{2\pi c} \frac{e^{i\frac{\omega}{c}d_B}}{d_B} e^{i\frac{\omega}{2cd_B}|\vec{\rho}_2 - \vec{\rho}_s|^2} \right\} e^{-i\vec{\kappa} \cdot \vec{\rho}_s}$$

where  $\vec{\rho}_s$  is the transverse vector on the source plane. We have therefore propagated the field from the source to the  $\vec{\rho}_1$  plane and  $\vec{\rho}_2$  plane in arm A and arm B, respectively.

Substituting  $g_1^*(\vec{\rho}_1, \vec{\kappa})$  and  $g_2(\vec{\rho}_2, \vec{\kappa})$  into  $G_{12}^{(1)}(\vec{\rho}_1; \vec{\rho}_2)$  and completing the integral on  $d\vec{\kappa}$ , we obtain

$$G_{12}^{(1)}(\vec{\rho}_1; \vec{\rho}_2) = \int d\vec{\kappa} g_1^*(\vec{\rho}_1, \vec{\kappa}) g_2(\vec{\rho}_2, \vec{\kappa})$$

$$\propto \int d\vec{\rho}_s e^{-i\frac{\omega}{c}d_A} e^{-i\frac{\omega}{2cd_A}|\vec{\rho}_1 - \vec{\rho}_s|^2} e^{i\frac{\omega}{c}d_B} e^{i\frac{\omega}{2cd_B}|\vec{\rho}_2 - \vec{\rho}_s|^2} \quad (43)$$

If we chose the distances from the source to the two detectors equal ( $d_A = d_B$ ), the integral of  $d\vec{\rho}_s$  in Eq. (43) yields a point-point correlation,  $\delta(\vec{\rho}_1 - \vec{\rho}_2)$ , between the  $\vec{\rho}_1$  plane and the  $\vec{\rho}_2$  plane, while taking an infinite size of the source. Thus, after the integration of the bucket detector, the joint-detection counting rate is calculated as:

$$R_c(\vec{\rho}_2) \propto \int d\vec{\rho}_1 |A(\vec{\rho}_1)|^2 \delta(\vec{\rho}_1 - \vec{\rho}_2) = |A(\vec{\rho}_2)|^2 \quad (44)$$

where  $A(\vec{\rho}_1)$  is the aperture function of the object plane.

Thus we have successfully explained the experimental observation in terms of two-photon interference.

As we know  $G_{12}^{(1)}$  has a counterpart of  $\Gamma_{12}^{(1)}$  in classical optics, namely the first-order coherence function. Can we use classical interference to explain this phenomenon? In fact, the theory of statistical correlation of intensity fluctuations is not a “must” for explaining the second-order correlation of thermal radiation. Examining  $G^{(2)} = G_{11}^{(1)}G_{22}^{(1)} + |G_{12}^{(1)}|^2$  of thermal light, it is easy to find that the intensity fluctuation correlation corresponds to the second term of  $|G_{12}^{(1)}|^2$ .  $G_{12}^{(1)}$  characterizes the first-order coherence, i.e., the ability of observing first-order interference, of the fields  $E(\mathbf{r}_1, t_1)$  and  $E(\mathbf{r}_2, t_2)$ . Why don't we explain HBT in terms of classical interference, instead of the intensity fluctuation correlation? As we usually say: “people are always smarter than theory.” This time, however, people have been too smart (we lost 50 years)! There is a reason not to do that, because  $E(\mathbf{r}_1, t_1)$  and  $E(\mathbf{r}_2, t_2)$  would not interfere with each other in the case of HBT:  $E(\mathbf{r}_1, t_1)$  and  $E(\mathbf{r}_2, t_2)$  are measured by two photodetectors at distance. Maxwell's wave equation is a linear differential equation. If  $E(\mathbf{r}_1, t_1)$  and  $E(\mathbf{r}_2, t_2)$  are solutions of the wave equation then the resulting field of  $E(\mathbf{r}, t) = E(\mathbf{r}_1, t_1) + E(\mathbf{r}_2, t_2)$  is also a solution. However, to claim a solution of the wave equation or interference,  $E(\mathbf{r}_1, t_1)$  and  $E(\mathbf{r}_2, t_2)$  have to be physically superposed at a space-time point, as we usually do in an interferometer. For example, in the Youngs double slit experiment,  $E(\mathbf{r}_1, t_1)$  and  $E(\mathbf{r}_2, t_2)$  are the fields at the double slits in early times relative to the time of photodetection. The resulting field of  $E(\mathbf{r}, t) = E(\mathbf{r}_1, t_1) + E(\mathbf{r}_2, t_2)$  is physically added at the space-time point of the photodetection. In HBT and Scarcelli's experiment, however, the situation is different.  $E(\mathbf{r}_1, t_1)$  and  $E(\mathbf{r}_2, t_2)$  are never brought together; further more,  $E(\mathbf{r}_1, t_1)$  and  $E(\mathbf{r}_2, t_2)$  are measured by two distant photodetectors! What kind of interference is this?

It is interference, but a different type. Under the framework of Glauber's photodetection theory, we have provided a two-photon interference picture. It is the interference between two-photon amplitudes. Unfortunately, this concept has no counterpart in classical electromagnetic theory of light, unless one makes the theory nonlocal by assuming  $E(\mathbf{r}_1, t_1)$  and  $E(\mathbf{r}_2, t_2)$  are

addable nonlocally through the measurement of two photodetectors, or makes a concept such as the interference between [field A goes to  $D_1 \times$  field B goes to  $D_2$ ] and [field B goes to  $D_1 \times$  field A goes to  $D_2$ ], which does not make any sense under the framework of Maxwell electromagnetic wave theory of light.

To conclude this section: the two-photon imaging experiment of Scarcelli *et al.* has demonstrated that the ghost imaging of chaotic light is an interference phenomenon involving the superposition between indistinguishable two-photon alternatives, rather than statistical correlation of intensity fluctuations. The two-photon correlations are *observed in* the intensity fluctuations, however, they are *not caused by* the statistical correlation of the intensity fluctuations.

## A statement from the author

This article was originally prepared as lecture notes for my students. The lecture notes were turned into a review paper at the end of 2006. The main purpose of this article is to clarify the fundamental concepts of quantum imaging and to provide the basic knowledge of physics and necessary tools of mathematics, which are involved in quantum imaging, for the general physics and engineering community. The debate regarding the quantum or classical nature of quantum imaging is still ongoing and will probably endure for a while. In a sense, this is a debate that started 50 years ago since the discovery of HBT. In this article, we have emphasized the two-photon coherence nature of the quantum imaging phenomena. As usual, there are always different opinions [30]. Classical formalisms do exist, such as Eq. (1); such formalism, however, is far from capturing the essence of the phenomenon and may mislead us from the truth, as it has happened to the two-photon physics of thermal light. The interpretation in terms of two-photon coherence elegantly explains all of the features of the experiments carried out with both “quantum” and “classical” sources. For this reason, two-photon coherence seems more suitable for explaining the physics of quantum imaging.

## Appendix A: Fresnel diffraction-propagation

In Fig. A–1, the field is freely propagated from plane  $\sigma_0$  to plane  $\sigma$ . For imaging applications, it is convenient to describe such a propagation in the form of Eq. (5). In this Appendix, we evaluate the  $g(\vec{\kappa}, \omega; \vec{\rho}, z)$ , namely the Green’s function or the field transfer function, for free-space Fresnel propagation.

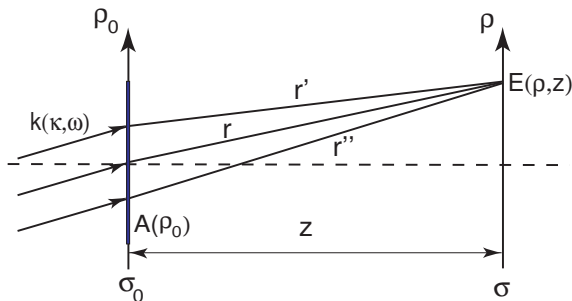


Figure A–1: Schematic of free-space Fresnel propagation. The complex aperture function  $\tilde{A}(\vec{\rho}_0)$  is composed by a real function  $A(\vec{\rho}_0)$  and a phase  $e^{-i\vec{\kappa} \cdot \vec{\rho}_0}$  associated with each of the transverse wavevector  $\vec{\kappa}$  on the plane of  $\sigma_0$ . Only one mode of wavevector  $\mathbf{k}(\vec{\kappa}, \omega)$  is shown in the figure.

According to the Huygens-Fresnel principle, the field at space-time point  $(\vec{\rho}, z, t)$  is the result of a superposition among these spherical secondary wavelets originated from each point on the  $\sigma_0$  plane, see Fig. A-1,

$$E(\vec{\rho}, z, t) = \int d\vec{\kappa} d\omega \tilde{E}(\vec{\kappa}, \omega) \int d\vec{\rho}_0 \frac{\tilde{A}(\vec{\rho}_0)}{r'} e^{-i(\omega t - \kappa r')} \quad (A-1)$$

where  $\tilde{A}(\vec{\rho}_0)$  is the complex aperture function and we have taken  $z_0 = 0$  and  $t_0 = 0$  as usual. We have also assumed a common complex amplitude  $\tilde{E}(\vec{\kappa}, \omega)$  for all point sources of the secondary wavelets on the plane of  $\sigma_0$ . In a paraxial approximation, we take the first-order expansion of  $r'$  in terms of  $z$  and  $\vec{\rho}$

$$r' = \sqrt{z^2 + |\vec{\rho} - \vec{\rho}_0|^2} \simeq z \left( 1 + \frac{|\vec{\rho} - \vec{\rho}_0|^2}{2z^2} \right).$$

$E(\vec{\rho}, z, t)$  is thus approximated as

$$E(\vec{\rho}, z, t) \simeq \int d\vec{\kappa} d\omega \tilde{E}(\vec{\kappa}, \omega) \int d\vec{\rho}_0 \frac{\tilde{A}(\vec{\rho}_0)}{z} e^{i\frac{\omega}{z}z} e^{i\frac{\omega}{2cz}|\vec{\rho} - \vec{\rho}_0|^2} e^{-i\omega t} \quad (A-2)$$

where  $e^{i\frac{\omega}{2cz}|\vec{\rho} - \vec{\rho}_0|^2}$  is named as the Fresnel phase factor.

Assuming the complex aperture function is composed by a real function  $A(\vec{\rho}_0)$  and a phase  $e^{-i\vec{\kappa} \cdot \vec{\rho}_0}$  associated with the transverse wavevector and the transverse coordinate on the plane of  $\sigma_0$ , which is reasonable for the setup of Fig. A-1,  $E(\vec{\rho}, z, t)$  can be written in the following form

$$E(\vec{\rho}, z, t) = \int d\vec{\kappa} d\omega \tilde{E}(\vec{\kappa}, \omega) e^{-i\omega t} \int d\vec{\rho}_0 A(\vec{\rho}_0) e^{i\vec{\kappa} \cdot \vec{\rho}_0} \frac{e^{i\frac{\omega}{c}z}}{z} e^{i\frac{\omega}{2cz}|\vec{\rho} - \vec{\rho}_0|^2}. \quad (A-3)$$

The Green's function for free-space Fresnel propagation is thus

$$g(\vec{\kappa}, \omega; \vec{\rho}, z) = \frac{-i\omega}{2\pi c} \frac{e^{i\frac{\omega}{c}z}}{z} \int_{\sigma_0} d\vec{\rho}_0 \tilde{A}(\vec{\rho}_0) e^{i\frac{\omega}{2cz}|\vec{\rho} - \vec{\rho}_0|^2} \quad (A-4)$$

where  $-i\omega/2\pi c$  is a normalization constant.

## Appendix B: Quantum state of thermal light

We assume a large number of atoms that are ready for two-level atomic transition. At most times, the atoms are in their ground state. There is, however, a small chance for each atom to be excited to a higher energy level and later release a photon during an atomic transition from the higher energy level  $E_2$  ( $\Delta E_2 \neq 0$ ) back to the ground state  $E_1$ . It is reasonable to assume that each atomic transition excites the field into the following state:

$$|\Psi\rangle \simeq |0\rangle + \epsilon \sum_{\mathbf{k}, s} f(\mathbf{k}, s) \hat{a}_{\mathbf{k}, s}^\dagger |0\rangle \quad (B-1)$$

where  $|\epsilon| \ll 1$  is the probability amplitude for the atomic transition. Within the atomic transition,  $f(\mathbf{k}, s) = \langle \Psi_{\mathbf{k}, s} | \Psi \rangle$  is the probability amplitude for the radiation field to be in the single-photon state of wave number  $\mathbf{k}$  and polarization  $s$ :  $|\Psi_{\mathbf{k}, s}\rangle = |1_{\mathbf{k}, s}\rangle = \hat{a}_{\mathbf{k}, s}^\dagger |0\rangle$ .

For this simplified two-level system, the density matrix that characterizes the state of the

radiation field excited by a large number of possible atomic transitions is thus

$$\begin{aligned}
\hat{\rho} &= \prod_{t_{0j}} \left\{ |0\rangle + \epsilon \sum_{\mathbf{k}, \mathbf{s}} f(\mathbf{k}, s) e^{-i\omega t_{0j}} \hat{a}_{\mathbf{k}, \mathbf{s}}^\dagger |0\rangle \right\} \\
&\times \prod_{t_{0k}} \left\{ \langle 0| + \epsilon^* \sum_{\mathbf{k}', s'} f(\mathbf{k}', s') e^{i\omega' t_{0k}} \langle 0| \hat{a}_{\mathbf{k}', s'} \right\} \\
&\simeq \left\{ |0\rangle + \epsilon \left[ \sum_{t_{0j}} \sum_{\mathbf{k}, \mathbf{s}} f(\mathbf{k}, s) e^{-i\omega t_{0j}} \hat{a}_{\mathbf{k}, \mathbf{s}}^\dagger |0\rangle \right] + \epsilon^2 [\dots] \right\} \\
&\times \left\{ \langle 0| + \epsilon^* \left[ \sum_{t_{0k}} \sum_{\mathbf{k}', s'} f(\mathbf{k}', s') e^{i\omega' t_{0k}} \langle 0| \hat{a}_{\mathbf{k}', s'} \right] + \epsilon^{*2} [\dots] \right\}
\end{aligned} \tag{B-2}$$

where  $e^{-i\omega t_{0j}}$  is a random phase factor associated with the  $j$ th atomic transition. Since  $|\epsilon| \ll 1$ , it is a good approximation to keep the necessary lower-order terms of  $\epsilon$  in Eq.(B-2). After summing over  $t_{0j}$  ( $t_{0k}$ ) by taking all its possible values, approximately, we have

$$\begin{aligned}
\hat{\rho} &\simeq |0\rangle \langle 0| + |\epsilon|^2 \sum_{\mathbf{k}, \mathbf{s}} |f(\mathbf{k}, \mathbf{s})|^2 |1_{\mathbf{k}, \mathbf{s}}\rangle \langle 1_{\mathbf{k}, \mathbf{s}}|, \\
&+ |\epsilon|^4 \sum_{\mathbf{k}, \mathbf{s}} \sum_{\mathbf{k}', \mathbf{s}'} |f(\mathbf{k}, \mathbf{s})|^2 |f(\mathbf{k}', \mathbf{s}')|^2 |1_{\mathbf{k}, \mathbf{s}} 1_{\mathbf{k}', \mathbf{s}'}\rangle \langle 1_{\mathbf{k}, \mathbf{s}} 1_{\mathbf{k}', \mathbf{s}'}|.
\end{aligned} \tag{B-3}$$

## References

- [1] A. Einstein, B. Podolsky, and N. Rosen, Phys. Rev. **35**, 777 (1935).
- [2] T.B. Pittman, Y.H. Shih, D.V. Strekalov, and A.V. Sergienko, Phys. Rev. A **52**, R3429 (1995).
- [3] D.N. Klyshko, Usp. Fiz. Nauk, **154**, 133 (1988); Sov. Phys. Usp, **31**, 74 (1988); Phys. Lett. A, **132**, 299 (1988).
- [4] Y.H. Shih, IEEE J. of Selected Topics in Quantum Electronics, **9**, 1455 (2003).
- [5] J.C. Howell *et al.*, Phys. Rev. Lett., **92**, 210403 (2004).
- [6] M. D'Angelo, Y.H. Kim, S. P. Kulik, and Y.H. Shih, Phys. Rev. Lett. **92**, 233601 (2004).
- [7] M. D'Angelo, A. Valencia, M.H. Rubin, and Y.H. Shih, Phys. Rev. A **72**, 013810 (2005).
- [8] D.V. Strekalov, A.V. Sergienko, D.N. Klyshko and Y.H. Shih, Phys. Rev. Lett., **74**, 3600 (1995).
- [9] A.N. Boto *et. al.*, Phys. Rev. Lett., **85**, 2733 (2000).
- [10] M. D'Angelo, M.V. Chekhova, and Y.H. Shih, Phys. Rev. Lett., **87**, 013603 (2001). Note: Due to the lack of a two-photon absorber, the joint-detection measurement in this experiment was on the Fourier transform plane rather than on the image plane. It might be helpful to point out that the observation of sub-wavelength interference in a Mach Zehnder type interferometer cannot lead to sub-diffraction-limited images, except a set of double modulated interference pattern. The Fourier transform argument works only for imaging setups as is in this experiment.
- [11] R.J. Glauber, Phys. Rev. **130**, 2529 (1963); Phys. Rev. **131**, 2766 (1963).



- [12] R.S. Bennink, S.J. Bentley, and R.W. Boyd, Phys. Rev. Lett. **89**, 113601 (2002); R.S. Bennink, *et al.*, Phys. Rev. Lett., 033601 (2004).
- [13] A. Gatti, E. Brambilla, M. Bache and L.A. Lugiato, Phys. Rev. A **70**, 013802, (2004).
- [14] K. Wang, D. Cao, quant-ph/0404078; D. Cao, J. Xiong, and K. Wang, quant-ph/0407065.
- [15] Y.J. Cai, and S.Y. Zhu, quant-ph/0407240, Phys. Rev. E, **71**, 056607 (2005).
- [16] R. Hanbury-Brown, and R.Q. Twiss, Nature, **177**, 27 (1956); **178**, 1046, 1447 (1956); R. Hanbury-Brown, *Intensity Interferometer*, Taylor and Francis Ltd, London, 1974.
- [17] A. Valencia, G. Scarcelli, M. D'Angelo, and Y.H. Shih, Phys. Rev. Lett. **94**, 063601 (2005).
- [18] G. Scarcelli, V. Berardi, and Y.H. Shih, Phys. Rev. Lett., **96**, 063602 (2006).
- [19] F. Ferri, *et al.*, Phys. Rev. Lett. **94**, 183602 (2005).
- [20] D. Zhang *et al.*, Opt. Lett., **30**, 2354 (2005).
- [21] M. H. Rubin, Phys. Rev. A **54**, 5349, (1996).
- [22] J. W. Goodman, *Introduction to Fourier Optics*, McGraw-Hill Publishing Company, New York, NY, 1968.
- [23] D.N. Klyshko, *Photon and Nonlinear Optics*, Gordon and Breach Science, New York, 1988.
- [24] Even if assuming a perfect lens without chromatic aberration, Fresnel diffraction is wave-length dependent. Hence, large broadband ( $\Delta\omega \sim \infty$ ) would result in blurred images in classical imaging. Surprisingly, the situation is different in quantum imaging: no aberration blurring.
- [25] G. Scarcelli, A. Valencia, and Y.H. Shih, Europhys. Lett. **68**, 618 (2004).
- [26] A popular perception views the two-photon phenomenon as the correlation between identical copies of “speckles” across the two light beams. Is this idea incorrect? One may simply split an attenuated (to single-photon’s level) or scattered laser beam into two by a beam-splitter to observe identical “speckles” either temporally or spatially on the two beams and yet, in this situation, the second-order correlation is a constant. On the other hand, for a smooth bright thermal light beam, which is achievable easily and classically, one may not be able to observe any “speckles”, the HBT two-photon correlation is still observable.
- [27] U. Fano, Am. J. Phys. **29**, 539 (1961).
- [28] M.O. Scully and M.S. Zubairy, *Quantum Optics* (Cambridge University Press, 1997).
- [29] W. Martienssen and E. Spiller, Am. J. Phys. **32**, 919 (1964).
- [30] A. Gatti *et al.*, Phys. Rev. Lett., **98**, 039301 (2007)(comment); G. Scarcelli, V. Berardi, and Y.H. Shih, Phys. Rev. Lett., **98** 039302 (2007)(reply).